Bioinspired scaffolds based on aligned polyurethane nanofibers mimic tendon and ligament fascicles

Saeid Bahrami, Hamid Mirzadeh, Atefeh Solouk, Delphine Duprez

Bioinspired scaffolds based on aligned polyurethane nanofibers mimic tendon and ligament fascicles

Saeid Bahrami [1,2], Hamid Mirzadeh [1], Atefeh Solouk [1*], Delphine Duprez [2**]

[1] Department of Biomedical Engineering, Amirkabir University of Technology (Tehran Polytechnic), Tehran, Iran

[2] Institut Biologie Paris Seine-Laboratoire de Biologie du Développement, Centre National de la Recherche Scientifique (CNRS) UMR 7622, Institut National de la Santé Et de la Recherche Médicale (Inserm) U1156, Université Pierre et Marie Curie, Sorbonne Université, Paris, France

Abstract

Topographical factors of scaffolds play an important role in regulating cell functions. Although the effects of alignment topography and 3D configuration of nanofibers as well as surface stiffness on cell behavior have been investigated, there are relatively few reports that attempt to understand the relationship between synergistic effects of these parameters and cell responses. Herein, the influence of biophysical and biomechanical cues of electrospun polyurethane scaffolds on mesenchymal stem cells (MSCs) activities was evaluated. To this aim, multiscale bundles were developed by rolling up the aligned electrospun mats mimicking the fascicles of tendons/ligaments and other similar tissues. Compared to mats, the 3D bundles not only maintained the desirable topographical features (i.e., fiber diameter, fiber orientation, and pore size), but also boosted tensile strength (~40 MPa), tensile strain (~260%), and surface stiffness (~1.75 MPa). Alignment topography of nanofibers noticeably dictated cell elongation

Correspondence:

* Atefeh Solouk, Department of Biomedical Engineering, Amirkabir University of Technology (Tehran Polytechnic), Tehran 1591634311, Iran. Email: atefeh.solouk@aut.ac.ir

** Delphine Duprez, Institut Biologie Paris Seine-Laboratoire de Biologie du Développement, Centre National de la Recherche Scientifique (CNRS) UMR 7622, Institut National de la Santé Et de la Recherche Médicale (Inserm) U1156, Université Pierre et Marie Curie, Sorbonne Université, Paris 75005, France. Email: delphine.duprez@sorbonne-universite.fr

This article has been accepted for publication and undergone full peer review but has not been through the copyediting, typesetting, pagination and proofreading process, which may lead to differences between this version and the Version of Record. Please cite this article as doi: 10.1002/biot.202300117.

and a uniaxial orientation, resulting in tenogenic commitment of MSCs. MSCs seeded on the bundles expressed higher levels of tenogenic markers compared to mats. Moreover, the biomimetic bundle scaffolds improved synthesis of extracellular matrix components compared to mats. These results suggest that biophysical and biomechanical cues modulate cell-scaffold interactions, providing new insights into hierarchical scaffold design for further studies.

KEYWORDS: biophysical cue, biomechanical cue, alignment topography of nanofibers, 3D configuration of nanofibers, surface stiffness, electrospun multiscale polyurethane scaffold

---

Abbreviations: 2D, two-dimensional; 3D, three-dimensional; DNA, deoxyribonucleic acid; ECM, extracellular matrix; EPU, electrospun polyurethane; GAG, glycosaminoglycan; MSCs, mesenchymal stem cells; PU, polyurethane; SEM, scanning electron microscopy; TCP, tissue culture plate.

1. INTRODUCTION

Partial or complete damage of tendon and ligament tissues can be treated via the repair, replacement, or regeneration of the tissue [1]. Most commonly, autografts, allografts, and xenografts are used in clinical but do not offer satisfactory long-term clinical outcomes owing to limitations such as re-rupture, an inadequate number of donors, inflammatory response, donor site morbidity, adhesion formation, mechanical mismatch, and infection risk [2,3].

Tissue engineering has contributed alternative strategies to develop regeneration of damaged tissues, with the most promising ones being those mimicking the native tissues as closely as possible [4]. One critical aspect in this context is the appropriate design of fibrous scaffolds that mimic the fibrillary architecture, mechanical and functional characteristics of the extracellular matrix (ECM) of native tissues [2]. Many native tissues such as tendons, ligaments, nerve, cardiac, and skeletal muscles are composed of a hierarchical construct of aligned nanoscale fibrils that are organized into microscale bundles containing both ECM and cellular components [5,6]. It is well known that the microstructure of the scaffold is fundamental to direct cell behavior [7].

Another important aspect in this context is to fabricate a tissue construct with comparable mechanical properties to native tissues.

Several manufacturing approaches have been employed, such as braiding, weaving, and knitting, to produce fibrous scaffolds inspired to native tissues [8]. Although such textile-based scaffolds could successfully combine controlled morphological (e.g., size and shape) and mechanical properties, they are in form of microfibrous bundles, which differ from the inherent nanoscale organization of collagen fibrils in native tissues [2]. Therefore, these microfibrous structures inevitably lead to reduced cellular activity and poor tissue healing [9]. With the introduction of nanoscale fibers, a new generation of scaffolds with superior properties has been emerged [10].

Among the technologies producing nanofibers, electrospinning is the most promising. Besides the several advantages of electrospun mats, which are defined and specified in the literature (e.g., similarity to the native ECM, high surface area to volume ratio, cost-efficient, simplicity, and ability to use various materials), developing the hierarchical scaffolds render this technique very attractive [11–13]. Furthermore, there is evidence that the alignment topography of electrospun nanofibers directs cells to specific phenotypes [14].

Fabricating fibrous bundles has attracted noticeable attention as they can be processed into different structures including woven, knitted, or braided constructs representing their potential to create a wide variety of highly biocompatible scaffolds with tailorable mechanical properties and architecture [10]. Although electrospun mats mimic the ECM matrix, these structures are considered as a single two-dimensional (2D) membrane and are not comparable to the native tissue bulk, which is a hierarchical three-dimensional (3D) construct [15]. Moreover, it has been well established that a fibrous bundle exhibit greater mechanical strength than single nanofibers or nanofibrous mats [9]. It has also reported that the 3D electrospun bundles support cell activities [1,16].

So far, different approaches have been applied to collect the electrospun bundles. Bosworth and colleagues have performed a series of studies on 3D bundles obtained by electrospun mats [15,17,18]. They evaluated the effect of different resorbable materials and cell culture conditions to provide the required mechanical properties and direct cell behavior [15,17,18]. In another attempt, researchers studied the multiscale bundles

obtained by rolling up portions of electrospun mats on a drum collector. For instance, Pauly et al. evaluated the impact of fiber orientation and geometry of poly(caprolactone) scaffolds for ligament tissue engineering [19]. Similarly, Sensini and coworkers reported the novel bundle scaffolds based on different materials to mimic human tendon fascicles in terms of morphological, mechanical, and biological properties [20–22]. They proposed a platform based on grouping the bundles to develop multiscale hierarchical structures, which mimic the tendon and ligament tissues [5,7,23]. Similarly, a tri-phasic fibrous scaffolds were developed, presenting a wavy intermediate zone and two aligned uncurled extremes [24]. In vivo studies proved a superior response of such triphasic scaffolds with a higher cell infiltration and a rich ECM deposition that presented also the characteristic alignment observed on the native tissues [24]. Another attempt corresponds to the work carried out by Laranjeira et al., who fabricated the bundles using wet electrospinning and employed textile technologies to enable the scalable production of the nanofibrous 3D hierarchical scaffolds with tailored dimensions [25].

To fabricate a biomimetic scaffold with desirable mechanical properties, polyurethanes (PUs) are promising materials [26]. PU-based constructs including electrospun PU (EPU) nanofibers, as biocompatible scaffolds, have extensively studied as scaffold for various biomedical applications [27]. A composite of EPU nanofibers incorporated with graphene was previously developed for cardiovascular applications [28]. Gotti and coworkers reported a novel approach to obtain artificial muscles based on EPU bundles [6].

It has been well established that the way cells modulate their behavior represents their interplay with the underlying substrate, not only by means of surface topography but also through surface stiffness and chemistry [4]. Hence, strategies employing the combination of all these factors are likely to promote a more desirable response toward tissue regeneration when the cell niche is mimicked as closely as possible [4]. Although efforts toward developing nanofibrous bundles through an electrospinning process have been conducted recently, there have been relatively few studies on the synergistic effects of such scaffolds on cell activities. To date, the relative roles of biophysical (i.e., alignment topography and 3D configuration of nanofibers) and biomechanical cues (i.e., surface stiffness) in the interactions between mesenchymal stem cells (MSCs) and

scaffolds are not well studied. The present study reports an approach to develop an innovative EPU-based multiscale nanofibrous structure aimed at mimicking the architecture and mechanical properties of fascicle of tendons and ligaments. Electrospun scaffolds based on polyurethane, namely EPU mats and EPU bundles with alignment topography of nanofibers, were fabricated and the effect of manipulating the biophysical and biomechanical cues on material properties and cell-scaffold interactions was evaluated. The proposed biomimetic structure might pave the way for future research in the context of tissue engineering.

2. MATERIALS AND METHODS

2.1. Materials

MDI-polyester/polyether polyurethane (CAS number: 68084-39-9), tetrahydrofuran (THF), and dimethylacetamide (DMAC) were purchased from Sigma-Aldrich (Germany). Dulbecco's modified Eagle's medium (DMEM), trypsin-EDTA, antibiotics (penicillin/streptomycin), fetal bovine serum (FBS), phosphate buffered saline (PBS), Dulbecco's phosphate buffered saline (DPBS), and glutaraldehyde (GTA) were purchased from Gibco (USA). Deionized water was used throughout.

2.2. Sample preparation

To make the aligned PU nanofibers, electrospinning was performed using a conventional setup (SBS, NanoAzma Co., Iran), as previously reported [29]. Briefly, the solution was prepared by dissolving PU at a concentration of 9% (w v^{-1}) in a mixed solvent of THF:DMAC = 3:2 (v v^{-1}). The solution was loaded into a syringe with a 21-gauge (21-G) needle, charged with a voltage of 15 kV, and fed at a rate of 1.0 mL h^{-1}, using a syringe pump. A rotating mandrel, which had a 10 cm diameter and was located at a distance of 10 cm from the needle, was utilized to collect the nanofibers. A rotating speed of 1500 rpm (peripheral speed = 7.9 m s^{-1}) was used to fabricate aligned nanofibers. The process was performed at room temperature.

To fabricate a multiscale bundle structures, the EPU mats were cut circumferentially into strips, and then manually rolled up to produce the 3D bundles. Therefore, the length of the final bundle was the same as the circumference of the rotating collector (~ 32 cm) and was made of nanofibers predominantly aligned in the direction of collector

rotation. A desirable diameter of bundles could be obtained by adjusting the time of electrospinning and the width of the strips to be rolled up.

The aforementioned experimental steps for the preparation of EPU mats and EPU bundles were schematically illustrated in Figure 1A. Digital images of the final scaffolds were also shown in Figure 1B,C.

2.3. Structural characterization

2.3.1. Morphology

The morphology of EPU mats and EPU bundles were examined via a high-resolution field emission scanning electron microscopy (FE-SEM; GeminiSEM500, Zeiss, Germany) at an accelerating voltage of 3 kV. Before imaging, the dried samples were mounted on the aluminium stubs with double-sided carbon tape and a thin layer of platinum coated on them using Leica ACE600 cryo-sputter coater.

Image J software (National Institutes of Health, USA) was used to measure the fiber diameter, bundle diameter, fiber orientation (relative to the horizontal axis), and pore size of the specimens using the SEM images. To this aim, at least 100 fibers or pores and 20 bundles were randomly selected in SEM. The porosity of the scaffolds was measured by determining the volume (V) and mass (m) of the scaffolds. Porosity of scaffolds was calculated as:

Porosity (%) = $(1- (\rho_s/\rho_{PU})) \times 100$

where ρ_s and ρ_{PU} are the density of the scaffold and polyurethan (1.18 g cm^{-3}), respectively [6].

2.3.2. Macroscopic mechanical properties

The mechanical properties of the EPU mats and EPU bundles were performed using a uniaxial tensile tester (Instron 5566, USA). To prevent slipping during testing, the sample ends were securely placed inside a paper frame. The tests were performed with a load cell of 50 N (Instron, USA) capacity at a constant rate of 10 mm min^{-1} (resulting in a strain rate of 1% s^{-1} to simulate the physiological loading speed on the native tendon and ligament tissues [19]) until failure occurred. Cross-sectional area of different scaffolds was estimated from measurements made using a digital caliper. A number of 3

replicates were considered for each condition and mechanical properties were obtained from stress-strain curves. More details of mechanical testing protocol have been explained in the Supporting Information.

2.3.3. Surface stiffness

The surface stiffness of scaffolds was determined in the wet state using a Chiaro nanoindenter system (Optics 11, Amsterdam, The Netherlands). A spherical indentation tip with a tip radius of 8.0 μm and a spring constant of 204.3 N m^{-1} was used to probe samples immersed in PBS at 37 °C for 24 h up to an indentation depth of 10 μm. The scaffolds was fixed on a glass slide and measurement was carried out at several different locations on surface of samples. Using the Hertzian model, the surface stiffness/elastic modulus value was calculated from the slope of the force-displacement curves in the region 15%–20% of maximum load using DataViewer 2.2 Software (Optics 11, Amsterdam, The Netherlands). Before testing, the optical sensitivity and geometrical factors were calibrated by indenting a hard surface (e.g., a glass slide). Before doing indentation on the scaffold, the calibration of the optical sensitivity and geometrical factors was done using a glass slide to locate the indentation site properly.

2.4. Biological evaluation

2.4.1. Serum protein adsorption

Samples were sterilized and transferred to microtubes containing 3 mL DMEM supplemented with 10% FBS and 100 units mL^{-1} penicillin-streptomycin followed by incubation at 37 °C with 5% CO_2. After 24 h, the scaffolds were retrieved, washed mildly in PBS (pH 7.4) thrice. 500 μL of 1% (w v^{-1}) SDS as elution buffer was used to solubilize adsorbed serum proteins on EPU scaffolds. Total amount of adsorbed protein was quantified using Bicinchoninic acid (BCA) assay (Pierce™, Thermo Scientific) according to the manufacturer's protocol. Briefly, 25 μL of extraction buffer with 200 μL of BCA working reagent (Reagent A:Reagent B in 50:1 ratio, respectively) were added into 96 well plate and incubated at 37 °C for 30 min. Absorbance was measured using a microplate reader (Varioskan LUX, Thermo Fisher Scientific, Waltham, MA, USA) at 562 nm. The optical density readings obtained were compared against a BSA standard graph corresponding to the amount of adsorbed protein.

2.4.2. Cell culture

For biological studies, the samples were prepared following several steps. First, the electrospun scaffolds were cut into 1×1 cm^2 (mats) and 1.5 cm (bundles), respectively. Second, the bundles were fixed on 6-well plate using the glue. Third, scaffolds were sterilized with 70% ethanol for 1 h, followed by repeatedly washing with DPBS. Finally, C3H10T½ cells, mouse cell line of mesenchymal stem cells (MSCs) [30], were seeded on the electrospun samples at a density of 5×10^4 cells/sample and allowed to adhere at 37 °C for 4 h. When the majority of cells adhered on the surface of samples, the culture medium containing DMEM, 10% FBS, and 1% penicillin/streptomycin was added into each well, and samples were further cultured for 7 days at 37 °C, 5% CO_2 in a humidified incubator. The culture medium was changed twice a week. Moreover, cells cultured on tissue culture plate (TCP) were considered to be the control group.

2.4.3. Cell morphology

The morphological and organization of MSCs on electrospun scaffolds were performed and analyzed using immunofluorescence images after 7 days of culture. Samples were rinsed twice gently with DPBS and then fixed with 4% paraformaldehyde overnight at 4 °C. After fixation, samples were rinsed gently with DPBS three times and then stained using Alexa Fluor 488 phalloidin (Life Technologies, USA) and 4',6'-diamidino-2-phenylindole hydrochloride (DAPI; Life Technologies, USA) at room temperature. The fluorescence images were taken by using a confocal laser scanning microscope (CLSM; LSM 980, Zeiss, Germany).

2.4.4. Cell infiltration

To investigate cell infiltration, MSCs seeded scaffolds were cultured for 7 days followed by the process explained in section 2.4.3.

2.4.5. Cell viability and proliferation

Metabolic activity of both electrospn acsffolds were evaluated for cell viability and proliferation using Alamar Blue® assay after 4 and 7 days of culture. At selected time points, the samples were transferred into fresh well plates containing complete medium with 10% Alamar Blue® and incubated for 4h. About 300 mL of the medium was then extracted from each sample and measured at 570/600 nm excitation/emission

wavelength in a fluorescent microplate reader (Varioskan LUX, Thermo Fisher Scientific, Waltham, MA, USA). More details have been explained in Supporting Information.

2.4.6. Biochemical assays

Samples from each treatment group (EPU mat, EPU bundle, and TCP) were washed in PBS and digested overnight in a papain digestion buffer (125 μg mL^{-1} of papain in DPBS with 2 mM of Na_2-EDTA and 2 mM of cysteine-HCl at pH 6.5) at 60 °C.

2.4.6.1. DNA content

The double-stranded DNA (dsDNA) content was quantified using Quant-iT PicoGreen dsDNA assay kit (Invitrogen, Cat. No. p11496) according to the manufacturer's instructions. Fluorescence was measured using a microplate reader (Varioskan LUX, Thermo Fisher Scientific, Waltham, MA, USA) at the excitation and emission wavelengths of 485 and 535 nm, respectively. A standard curve was generated to correlate the DNA content with fluorescence intensity.

2.4.6.2. Glycosaminoglycan content

Sulfated glycosaminoglycan (GAG) content were quantified spectrophotometrically using the Blyscan kit, according to manufacturer's instructions (Biocolor, Carrickfergus, United Kingdom). This assay is based on the specific binding of the cationic dye 1,9-DMMB to the sulfated GAG chains of proteoglycans and protein-free sulfated GAG chains. Briefly, standard solutions (0, 1.0, 2.0, 3.0, and 5.0 μg of chondroitin-4-sulfate in 100 μL) and test samples (300 μL) were mixed with 300 μL of Blyscan dye reagent for 30 min at room temperature resulting in GAG-dye complex formation, which was recovered by centrifugation for 10 min at 12000 rpm. Then, the pellets were resuspended in 300 μL of dissociation buffer. Absorbance was measured at 656 nm in a microplate reader (Varioskan LUX, Thermo Fisher Scientific, Waltham, MA, USA). The measurement was carried out through comparison with a standard curve generated with bovine tracheal chondroitin 4-sulfate dissolved at a series of known concentrations that mentioned above.

2.4.6.3. Collagen content

Total collagen was determined using a modified hydroxyproline assay. Briefly, 100 µL of each sample was hydrolyzed overnight using an equal volume of concentrated hydrochloric acid (6 N HCl) at 120 °C. A specific volume of sample and standard was transferred to 96-well plate and incubated in 60 °C to dry. Then, 100 µL chloramine T/oxidation buffer was added to each well and allowed to stand at room temperature for 5 minutes. The solution was combined with 100 µL diluted DMAB reagent and placed in a 60 °C for 90 minutes. Absorbance was read at 560 nm a microplate reader (Varioskan LUX, Thermo Fisher Scientific, Waltham, MA, USA). The hydroxyproline content was calculated from a calibration curve based on standard solutions and converted to collagen using a conversion factor of 1:7.46 (hydroxyproline:collagen) [31].

2.4.7. Gene expression

QIA-Shredder and RNeasy mini-kits (QIAgen, USA) were used to extract total cellular RNA from cell-seeded samples, according to the manufacturer's instructions. Equal amounts of total RNA, approximately 500 ng, were then reverse transcribed to cDNA, using a High Capacity cDNA Reverse Transcription kit (Applied Biosystems, California, USA) according to the manufacturer's protocol. RT-qPCR analysis was performed in a StepOnePlus™ Real-Time PCR System (Thermo Scientific) using SYBR Green PCR Master Mix (Applied Biosystems). Expression of collagen types 1 (*Col1a1*) and 2 (*Col2a1*), scleraxis (*Scx*), tenascin C (*Tnc*), tenomodulin (*Tnmd*), osteocalcin (*Bglap*), osterix (*Sp7*), and SRY-Box 9 (*Sox9*) was evaluated. Threshold cycle (CT) values were corrected for efficiency and normalized to expression of 18s rRNA (*Rn18S*) as the internal control. Relative gene expression was normalized to TCP (control) and measured using comparative Ct ($2^{-\Delta\Delta Ct}$) method [32]. More details including the targets and sequences of primers have been explained in Supporting Information.

2.5. Statistical analysis

All measurements were performed at least in triplicates and data are presented as the mean ± SD (standard deviation). Statistical analysis was carried out with GraphPad Prism version 9 software (California, USA). Results were analyzed for significant differences using Student's t-test and one-way ANOVA. The p-value < 0.05 was

considered to be statistically significant. Statistically significant values are presented as *$p < 0.05$, **$p < 0.01$, ***$p < 0.001$, and ****$p < 0.0001$.

3. RESULTS

3.1. Structural characterization

3.1.1. Morphology

In order to mimic the multiscale structure of the fascicle of tendons and ligaments, firstly aligned EPU mats were fabricated and then, single bundle structure were constructed by rolling up the EPU mats (Figure 1). To obtain the aligned nanofibers, a high rotating speed of the collector (i.e., 1500 rpm) was used according to methods published elsewhere [29]. After 5 h of electrospinning, the thickness of EPU mat was ~100 μm. By fixing the time of electrospinning and the width of the strips to be rolled up, bundles with a diameter of ~500–600 μm were obtained.

The microstructure of the scaffolds was studied using SEM (Figure 2A,B). The aligned nanofibers in both EPU mats and EPU bundles were homogeneous, smooth, continuous, and with no defects such as beads. The alignment of nanofibers was analyzed on both EPU mats and EPU bundles using the SEM images (Figure 2A,B). As expected, a preferential orientation of the nanofibers in one specific direction was observed in both constructs. In electrospun mats, about 72% of nanofibers were oriented in the range of 70-100°, and similar observation was found in the range of 140-170° for the bundles. The mean diameter of aligned nanofibers was 547.30±101.57 nm and 558.85±164.55 nm for mats and bundles, respectively. Moreover, the diameter of bundles was 558.27±44.55 μm (Figure 2C).

The mean pore size was measured using the SEM images (Figure 2D). The EPU mats possessed a mean pore size of 16.94±5.33 μm, which was not significantly different compared to that of EPU bundles (16.34±6.50 μm). In addition, the results indicated a higher value of density of EPU bundles (0.89±0.10 g cm^{-3}) compared to the EPU mats (0.64±0.13 g cm^{-3}) (Figure 2E). Inversely, the porosity of EPU bundles (~25%) was significantly lower than that of EPU mats (~45%).

3.1.2. Macroscopic mechanical properties

Mechanical performance is one of the essential requirements to ensure that an engineered scaffold would be successful for clinical applications [33]. Uniaxial tensile testing was performed on both EPU mats and EPU bundles, along the nanofibers direction (Figure 3A).

The typical stress-strain curves of both constructs demonstrated a slight toe region before the linear elastic region. Nanofibers configuration, whether the construct was a mat or a bundle, demonstrated a statistical effect on mechanical properties; EPU bundles had higher failure stress, failure strain, and work to failure than EPU mats ($p < 0.05$). In particular, the failure stress of EPU mats was 28.83±6.07 MPa, which increased meaningfully to 39.62±1.16 MPa in EPU bundles. Similarly, failure strain increased notably from 122.72±27.50% (mats) to 230.50±13.53% (bundles). The EPU bundles showed an increase in work to failure compared to the EPU mats (5.70±0.35 J mm^{-3} versus 2.07±0.83 J mm^{-3}). Meanwhile, no significant difference was observed between EPU mats and EPU bundles in tensile modulus (30.71±3.68 MPa versus 30.00±0.98 MPa), yield stress (19.21±1.67 MPa versus 18.51±1.98 MPa), yield strain (70.01±7.65% versus 68.61±6.69%), and work to yield (0.65±0.16 J mm^{-3} versus 0.62±0.12 J mm^{-3}).

3.1.3. Surface stiffness

The surface stiffness of scaffold is known as a biomechanical cue affecting cell functions [34]. The microindentation was performed to evaluate the micromechanical behavior of the electrospun EPU mats and EPU bundles incubated for 24 h at 37 °C. As shown in Figure 3B, the 3D bundle constructs demonstrated a stiffer substrate compared to 2D electrospun mats representing their potential to induce different cell responses [35]. More in details, the surface stiffness of bundles was approximately 1.75 MPa, which was 75% higher than that of electrospun mats (~1 MPa).

3.2. Biological evaluation

3.2.1. Protein adsorption

The cell-scaffold interactions are mediated by the proteins that adsorbed on the surface of scaffold; therefore, the protein adsorption behavior is a critical factor to evaluate the scaffolds for the tissue engineering applications [36]. In this direction, the serum protein adsorption on the electrospun constructs was investigated after 24 h incubation

at 37 °C using the BCA assay kit. Figure 4A shows the protein adsorption pattern obtained in both EPU mats and EPU bundles. Significant improvement in protein adsorption was observed in the bundle constructs. In particular, the protein adsorption ability of EPU bundles was 66.64±29.55 μg cm^{-2} representing over six-fold as that of 9.64±1.03 μg cm^{-2} for EPU mats.

3.2.2. Cell morphology

It is commonly accepted that manipulating the topographical factors of matrices could regulate cell behavior including cell morphology and orientation [37]. To determine the influence of alignment topography and 3D configuration of nanofibers on cell morphology, both seeded-scaffolds were stained after 7 days of culture. The cytoskeleton was stained red with FITC-conjugated phalloidin, and the nucleus was stained blue with DAPI.

As shown in fluorescent images (Figure 4B), MSCs were well attached to all samples but there was a meaningful difference in cell morphology depending on which substrate structure the cells were in contact with. Moreover, cells exhibited a stellate-patterned morphology and spread in random orientation on TCP (control), whereas for 2D and 3D aligned EPU nanofibers (i.e., mats and bundles scaffolds, respectively), cells displayed a spindle-patterned morphology with elongation and were oriented along the underlying fiber direction.

3.2.3. Cell infiltration

To evaluate the extent of cell infiltration into the scaffolds, MSCs grown on the samples were stained with phalloidin and DAPI. A series of confocal sections were acquired from the top surface along the z-axis with a CLSM (Figure 4C). Scanning the EPU mats and bundles with cells after 7 days revealed clear differences. The cells infiltrated into the initial layers of bundles and possessed a thick layer of cells around the outer circumference of the bundle, whereas the entire EPU mats were occupied by the cells.

3.2.4. Cell viability and proliferation

Cell viability is crucial to evaluate biocompatibility of scaffolds [38]. To this aim, the metabolic activity of MSCs was investigated on both scaffolds using Alamar Blue assay after 4 and 7 days of culture. As shown in Figure 4D, cell proliferation and cell number

increased over time in both samples. The results revealed a significant increase ($p < 0.0001$) in the metabolic activity for both types of scaffolds from day 4 to day 7. In addition, no significant differences were observed between conditions at each time point.

3.2.5. Biochemical assays

3.2.5.1. DNA content

The DNA content in each sample is recognized as an indicator of cell proliferation [39]. The DNA content of each sample was measured using PicoGreen assay after 7 days of culture (Figure 4E). The DNA of cells seeded on the TCP was used as control. The results demonstrated that there was no statistical differences in DNA content between different samples.

3.2.5.2. Glycosaminoglycan and collagen content

Synthesis and deposition of ECM components including proteins and proteoglycans by cells are important for tissue regeneration and remodeling [40]. In this regard, the total GAG and collagen content was detected on the three samples after 7 days of culture (Figure 4F,G). The matrix components synthesized by the cells seeded on the TCP was used as control.

MSCs seeded on different groups continuously accumulated ECM during the culture time. In addition, GAG and collagen synthesis were significantly higher in the case of bundle scaffolds than others. The total amount of GAG synthesis was ~1.75 ng ng^{-1} cm^{-2}, ~28.45 ng ng^{-1} cm^{-2}, and ~2.21 ng ng^{-1} cm^{-2} for EPU mats, EPU bundles, and TCP (control), respectively. Similarly, the level of collagen content was ~1.42 ng ng^{-1} cm^{-2}, ~25.96 ng ng^{-1} cm^{-2}, and ~2.60 ng ng^{-1} cm^{-2} for EPU mats, EPU bundles, and TCP (control), respectively.

3.2.6. Gene expression

The present electrospun scaffolds showed distinct nanofibrous configurations that might confer a specific cell phenotype. To this aim, the MSCs were seeded on the scaffolds and TCP (control) for 7 days and then RT-qPCR was performed to quantify the

expression of markers, including tendon/ligament-, cartilage- and bone-related markers (Figure 4H).

As shown in Figure 4H, one can notice an enhanced expression of tendon-related markers (i.e., *Col1a1*, *Scx*, *Tnc*, and *Tnmd*) in the aligned nanofibrous architecture versus TCP, while no significant difference was observed in the expression of cartilage-related marker (i.e., *Sox9*) and bone-related markers (i.e., *Bglap* and *Sp7*). Among the scaffolds, the multiscale EPU bundles induced tendon differentiation by promoting the expression of *Col1a1* and *Scx*.

4. DISCUSSION

Native tendon and ligament tissues exhibit a hierarchical structure from nano to macro scale based on collagen fibers arranged along their longitudinal axes [16]. This hierarchical structure plays a vital role in the structural and biological properties of native tissues [16]. Given that, in this study, multiscale fascicle-bioinspired bundles of axially aligned EPU nanofibers were developed by rolling up EPU mats (Figure 1). This approach resulted in production of aligned EPU bundles of several centimeters in length meaning that the process required no special tools and was similar to rolling up a membrane into a tube [19]. A comparison of EPU mats and EPU bundles in terms of fiber diameter, fiber orientation, and pore size suggested that the architecture of scaffolds remained intact after bundle fabrication (Figure 2).

The dimensions of both scaffolds, in terms of fiber and bundle diameter, are comparable to those found in the hierarchical organization of the fibrils and fascicles in the native tendons and ligament tissues [23]. Such tissues are comprised of collagen fibrils, which range from 50–500 nm in diameter [19]. Collagen fibrils are organized into fibers with diameters in the range of 10–50 μm [19]. Groups of fibers are then organized into fascicles with a size of 50–500 μm, which are combined to compose the whole tendon or ligament [19]. However, the diameters of subfascicles and fascicles vary significantly in different tendon and ligament types [41].

The pore size of scaffold is the fundamental characteristic to provide enough space for cell activities and the exchange of oxygen, nutrients, and metabolic waste [42]. The results of pore size for both EPU mats and EPU bundles are in the suitable range for

tissue engineering applications (Figure 2D) [43,44]. Additionally, the higher density of EPU bundles could be explained by the multilayer structure of such scaffolds, which resulted in fiber packing (i.e., fiber density) (Figure 2B and Figure 2E)[45]. The center of the nanofibrous bundles was not hollow, which could be accounted for the low thickness of electrospun mats that recognize as a 2D structure [46].

The mechanical testing confirmed that, in general, all samples demonstrated an initial highly-compliant toe region, which is similar to that of native tendon fascicles [20]. The results indicated that the EPU bundles showed a ductile behavior with higher values of failure stress, failure strain, and work to failure compared to the EPU mats (Figure 3A). The ductile behavior of the EPU bundles represents a safety factor in case of overload, which is a crucial requirement for orthopedic implants in strenuously loaded conditions [21]. This behavior can be attributed to the multilayer structure of constructs (i.e., denser fiber packing), which is shown in Figure 2B and Figure 2E. It suggests that a higher amount of nanofibers are oriented in parallel to the applied force and distribute the force, hence more loads are required to cause elastic deformation [19]. As previously explained, PU polymer was selected in the present study to fabricate the electrospun scaffolds as it can provides desirable mechanical properties [47]. The results confirmed that the structure of EPU bundle scaffolds with alignment topography of nanofibers contributes to the improvement in the mechanical properties, in consistent with previous studies [6,15,19]. Moreover, the aligned nanofibrous EPU mats demonstrated mechanical properties similar to those measured elsewhere [29]. It should be noted that standard clamps were used in this testing, which might have led to a slight under-estimate of the failure properties. But considering that the specimens did not fail in the clamp, it seems that such effects, if any, must have been negligible.

The mechanical properties of both constructs were promising and comparable to those of other PU-based grafts (e.g., Artelon® (SportMesh™)) or native tendon and ligament tissues (Table 1). For instance, the tensile strength of native tendons (e.g., human patellar, rotator, and Achilles) is in the range of few to several tens MPa [48], which corresponds to the range obtained for our samples. This finding could account for alignment topography and fiber diameter in nanoscale [19,49]. As mentioned above, when most nanofibers are oriented along to the applied force, they can distribute the force, meaning more loads requiring for elastic deformation [19]. It is also well

documented that there is generally an inverse relationship between fiber diameter and mechanical properties when it changes from micrometer to nanometer [49]. This change is probably due to the entanglement of nanofiber diameter in molecular levels, which results in fewer defects in the structure (i.e., more structural uniformity), and thus higher durability [50]. Although the yield and failure strain of scaffolds are higher than those of natural tendon and ligament tissues, which can be useful as a safety factor in case of an overload of the scaffold, it caused a relevant decrement in the tensile modulus of bundles compared to native tissues. This needs to be addressed in future works.

Sufficient mechanical properties are required for engineered scaffolds [51]. It becomes more important when the scaffolds are used to accelerate the healing of tissues such as tendons and ligaments, which are subjected to a high levels of force [52]. From a regeneration point of view, strength is a critical factor to maintain the structural integrity and mechanical properties of scaffolds during implantation and experiencing loads until sufficient regeneration of damaged tissue [53]. Furthermore, providing desirable mechanical support is critical for the newly deposition of ECM components at the injury site during tissue regeneration [16].

Increasing the surface stiffness of bundles in comparison to mats (Figure 3B) could be attributed to the possibility of intramolecular interactions between PU chains (i.e., hydrogen bonding and van der Waals) and more packing density (i.e., multilayer structure), which are shown in Figure 3C and Figure 2E, respectively [54,55]. It is well established that the crosslinking and hydrogen bonds restrain the polymer chain mobility, which is translated to the more rigidity and high surface stiffness [54]. As described in the literature, hydrogen bond in polyurethane can be identified as a hard-hard segment hydrogen bond (NH- - -O=C bond) and a hard-soft segment hydrogen bond (NH- - -O– bond) [56]. In addition, Doyle et al. showed that bundling of aligned collagen fibers led to more packing density of fibers and hence, increased surface stiffness [55]. However, further studies are required to understand this observation.

An artificial ECM not only affects cell shape but also the physical and mechanical properties of the ECM including surface stiffness contribute to cell behavior [57]. Cell adhesions are correlated to the adhesive force at the cell-matrix interface and regulated

by integrins associated with the assembly of focal adhesions [58]. It was found that the focal adhesion sizes increase with the stiffness of substrates meaning focal adhesions become more spread on stiff substrates compared to the soft substrate [59]. Furthermore, the cells that are attached to the underlying substrate, exert contractile forces, leading to tensile stresses in the cytoskeleton [34]. The relationship between these forces and the surface stiffness of the ECM can have a major impact on cell activities [57].

Higher protein adsorption on bundles than on mats (Figure 4A) could be ascribed to the higher surface stiffness of EPU bundles [60]. Cell adhesion onto the scaffolds is facilitated through a favored interplay between cells and scaffold, triggered mainly by cell receptors and ECM proteins [61]. In other words, the cell adhesion process is directly associated with protein adsorption on a scaffold, and therefore, any improvement in terms of protein adsorption pattern can be translated to increasing cell attachment [62]. Therefore, various surface modification approaches using peptides, proteins, and polymers have been investigated to improve protein adsorption, i.e., cell adhesion to substrates [63]. However, the effect of topographical architecture of scaffold on cell adhesion has not been well investigated [63]. Overall, given the fact that the cell adhesion process is directly associated with protein adsorption on a scaffold, it seems that the EPU bundle scaffold is likely to provide a better cell environment than EPU mats.

It was observed that EPU bundles benefited from the biophysical cues (i.e., alignment topography and 3D configuration of nanofibers) (Figure 2) similar to the native tissues. The importance of this observation becomes even more pronounced in cell-scaffold interactions [64]. A combination of these same features and synergistically applying them to the hierarchical structure can direct the cells to commit to the specific phenotype and/or avoid drift to non-desirable phenotypes [25]. Given that, MSCs displayed elongated morphology and aligned orientation on both mats and bundles (Figure 4B), which is in accordance with previous reports confirming that the cells recognize and respond to the topographical cues [65]. Regardless of different configurations and compositions of fibers, it has been well documented that fibrous scaffolds with anisotropic micro- and nanotopographies induce cytoskeletal reorganization and dictated cell elongation with high degrees of orientation [66]. The

results regarding cell orientation on scaffolds studied in this work were influenced by the structure-function relationship of such scaffolds and represent the importance of design strategy for developing a suitable scaffold to mimic the hierarchical structure of native tissues [34].

According to the results, the cells infiltrated through the whole depth of EPU mats and initial layers of EPU bundles (Figure 4C), which may be due to the lower thickness of the mats compared to the bundles. This finding highlighted the cell adhesion around the entire outer surface of scaffolds. In addition, this observation implies that after a certain period of cell culture, MSCs could infiltrate the entire scaffolds.

Alamar Blue assay showed that the scaffolds not only were cytocompatible but also supported cell proliferation (Figure 4D), which is a key requirement during the tissue regeneration process. This finding is consistent with our previous reports, which showed the biocompatibility of EPU nanofibers with different cell types (e.g., fibroblast and endothelial, and MSCs) [28,29].

A survey of the literature indicates that cell functions in the various matrices is affected by several factors: 1) biophysical cues like pore size and porosity, 2) biomechanical cues like surface stiffness, and 3) biochemical cues like surface chemistry and functional group of the substrate exposed to the cells [67,68]. Therefore, the higher amounts of collagen and GAG synthesis on EPU bundle (Figure 4F,G) could be ascribed to the biophysical, biomechanical, and biochemical cues of such scaffolds, i.e., 3D configuration of nanofibers, surface stiffness, and protein adsorption, respectively.

In the work carried out by Li et al., who investigated the effect of nanofiber configuration of electrospun scaffolds on phenotype and matrix synthesis of cells, the bundle scaffolds induced significantly more ECM deposition than mats, which highlights the critical roles of the biomimetic structure of bundles in promoting the maturation of engineered tissue constructs [69]. Similar results were reported by Rinoldi and coworkers, who fabricated the electrospun mats composites containing silica nanoparticles wherein a significant improvement of matrix deposition was attributed to the structure and surface stiffness of the constructs [70].

The proteins, like collagen, and proteoglycans are the main components of the ECM, which provide structural and mechanical integrity of native tissues [71]. Moreover, the

secretion of collagen and GAG during the cell-scaffold interactions are the major interest in regulating the biological function of native tissues [33]. The nanoscale fibers of both scaffolds positively affect the cell-scaffold interactions [72]. As such, the nanofibers imitate a matrix in the state of injury and the cells, hence, initiated a healing response by synthesis more matrix components, such as proteoglycans [64]. On the other hand, the scaffolds with larger fibers probably mimic the fibers of a healthy tissue matrix, and thus the cells reduce excess matrix deposition [64].

Although soluble factors are recognized to control cell fate, biophysical and biomechanical cues provide equally important instructions for guiding cell fate [64,69]. In this direction, the effect of such cues on gene expression was evaluated in the present work (Figure 4H). RT-qPCR results showed that both EPU mats and EPU bundles significantly improved the tenogenic differentiation of MSCs compared to the TCP. However, EPU bundles resulted in a higher expression of tendon-related markers in comparison with mats.

Several parameters affect gene expression by different cell types. Cells recognize and respond to contact guidance cues, which extend to nanoscale topographical features [37,57]. Such alignment topography of nanofibers is deemed to be an ideal substrate for facilitating the regeneration of tissues with similar structures, like tendons, ligaments, nerve, cardiac, and skeletal muscles, since they can convey topographical cues to cells and consequently promote higher expression of the corresponding markers, as reported by several researchers [2,73]. Thus, the promotion of MSCs toward tendon lineage on EPU mats and EPU bundles compared to TCP could be attributed to the alignment topography of nanofibers. In our previous research, the cell-scaffold interactions showed that MSCs expressed higher level of tendon-related markers, including *Col1a1*, *Col1a2*, *Scx*, and *Tnmd*, on aligned nanofibers compared to random ones or TCP [29].

According to the literature, two major factors play a profound role in the upregulation of tendon-related markers expression (i.e., *Col1a1* and *Scx*) on bundles versus mats. There is meaningful evidence endorsing the contribution of physical and mechanical properties of the matrix to stem cell fate, as described previously in the discussion of results corresponding to the surface stiffness [57]. Therefore, the significant difference in the expression of tendon-related markers on bundles versus mats may be linked to

their surface stiffness, which is in line with other reports [74,75]. For instance, in a work carried out by Islam et al., the effect of substrate stiffness on tenoinduction of human MSCs was reported [74]. The results showed higher expression of collagen type 1 on the stiffer substrate after 14 days of culture [74]. In another attempt, stiffer substrates induced higher expression of *Tnmd* compared to soft ones [75].

Moreover, the literature highlighted the influence of scaffold architecture on the direction of cellular commitment. In particular, the 3D configuration of bundles improved the expression of tendon/ligament-related markers and other native tissues with similar structures [16]. The combination of nanoscale and macroscale cues, which mimic the ultrastructure of native tissues (e.g., collagen fibrils and fibers/fascicles of tendons and ligaments) can synergistically induce the cells to specific phenotype related to anisotropic tissues [76]. For example, Xu and coworkers demonstrated that topographical and architectural cues of bundle scaffold act as strong inducers in the phenotypic expression levels of tendon-related genes [77]. Similar results was found in a study performed by Li et al. who seeded the cells on different constructs, including random and aligned electrospun mats and aligned electrospun bundles, and results proved the upregulation of meniscus-related genes on bundles [69].

Taken together, this work confirmed that fascicle-bioinspired EPU bundles possess suitable structural and biological properties for tendon/ligament tissue engineering. Such biophysical (alignment topography and 3D configuration of nanofibers) and biomechanical (surface stiffness) cues can facilitate tendon/ligament regeneration (Figure 5). There is high potential for the usage of EPU bundles in the development of hierarchical 3D aligned scaffolds for the construction of tissue-specific functional architecture and subsequently, advancing regenerative therapies for tissue repair. Although this study has targeted such structures for tendon/ligament fascicles, the results represent a platform for other tissues with similar structure (skeletal muscles, nerves, etc.).

5. CONCLUSION

The present study contributes to developing an innovative electrospun scaffold able to closely mimic the native architecture of anisotropic tissues such as tendon/ligament fascicles. The 3D bundles were prepared by rolling up the aligned EPU mats. The

synergistic effects of biophysical (alignment topography and 3D configuration of nanofibers) and biomechanical (surface stiffness) cues on the material and biological performance of both EPU mats and EPU bundles were evaluated. This approach allowed the fabrication of bundle constructs representing the structure with multiscale arrangement from nano to microscale. The material characterization proved the similarity of topographical cues (i.e., fiber diameter, fiber orientation, and pore size) in both constructs. The mechanical analysis revealed the higher failure stress, failure strain, and work to failure of multiscale bundles compared to mats. Moreover, the surface stiffness of bundles was notably higher than mats. The alignment topography of nanofibers in both scaffolds dictated a uniaxial orientation and elongated cell morphology. Both electrospun scaffolds supported cell proliferation over time with no cytotoxicity. Furthermore, the 3D configuration and surface stiffness of bundles meaningfully orchestrates cell-secreted ECM components, including collagen and GAGs. Although the alignment topography of nanofibers guided the MSCs to commit to tendon lineage, the structural feature of bundles boosted significantly more the expression of tendon-related markers. This study provides new insights into designing hierarchical scaffolds, which should further be investigated with complementary studies in an animal model to determine the suitability of such scaffolds for tissue engineering applications.

ACKNOWLEDGMENTS

The authors are thankful to Michaël Trichet from the IBPS electron microscopy core facility and the support of «Région Île-de-France», Sorbonne-Université and CNRS. We acknowledge Sophie Gournet and Mohammad Bagher Molaei for their help in illustrations. The authors would like to express their gratitude to the office of Professional Laboratories and Technology Services in Amirkabir University of Technology (Tehran Polytechnic) for supporting this research under grant number 1401-0506. Saeid Bahrami thanks for the support the partial PhD scholarship from the French Embassy in Iran and the Ministry of Science, Research, and Technology of Iran.

CONFLICT OF INTEREST STATEMENT

The authors declare no commercial or financial conflict of interest.

AUTHOR CONTRIBUTIONS

Saeid Bahrami: Conceptualization, Data curation, Formal analysis, Funding acquisition, Investigation, Methodology, Project administration, Resources, Software, Validation, Visualization, Writing - original draft, Writing - review & editing. **Hamid Mirzadeh:** Conceptualization, Funding acquisition, Investigation, Methodology, Project administration, Resources, Supervision, Validation, Writing - review & editing. **Atefeh Solouk:** Conceptualization, Funding acquisition, Investigation, Methodology, Project administration, Resources, Supervision, Validation, Writing - review & editing. **Delphine Duprez:** Conceptualization, Funding acquisition, Investigation, Methodology, Project administration, Resources, Supervision, Validation, Writing - review & editing.

DATA AVAILABILITY STATEMENT

The raw data will be made available upon request.

REFERENCES

[1] K.M. Ali, Y. Huang, A.Y. Amanah, N. Mahmood, T.C. Suh, J.M. Gluck, In vitro biocompatibility and degradation analysis of mass-produced collagen fibers, Polymers (Basel). 14 (2022). https://doi.org/10.3390/polym14102100.

[2] S. Wu, Y. Wang, P.N. Streubel, B. Duan, Living nanofiber yarn-based woven biotextiles for tendon tissue engineering using cell tri-culture and mechanical stimulation, Acta Biomater. 62 (2017) 102–115. https://doi.org/10.1016/j.actbio.2017.08.043.

[3] O. Evrova, G.M. Bürgisser, C. Ebnöther, A. Adathala, M. Calcagni, E. Bachmann, J.G. Snedeker, C. Scalera, P. Giovanoli, V. Vogel, J. Buschmann, Elastic and surgeon friendly electrospun tubes delivering PDGF-BB positively impact tendon rupture healing in a rabbit Achilles tendon model, Biomaterials. 232 (2020) 119722. https://doi.org/10.1016/j.biomaterials.2019.119722.

[4] H. Almeida, R.M.A. Domingues, S.M. Mithieux, R.A. Pires, A.I. Gonçalves, M. Gómez-Florit, R.L. Reis, A.S. Weiss, M.E. Gomes, Tropoelastin-coated tendon biomimetic scaffolds promote stem cell tenogenic commitment and deposition of elastin-rich matrix, ACS Appl. Mater. Interfaces. 11 (2019) 19830–19840. https://doi.org/10.1021/acsami.9b04616.

[5] A. Sensini, C. Gotti, J. Belcari, A. Zucchelli, M.L. Focarete, C. Gualandi, I. Todaro, A.P.

Kao, G. Tozzi, L. Cristofolini, Morphologically bioinspired hierarchical nylon 6,6 electrospun assembly recreating the structure and performance of tendons and ligaments, Med. Eng. Phys. 71 (2019) 79–90. https://doi.org/10.1016/j.medengphy.2019.06.019.

[6] C. Gotti, A. Sensini, G. Fornaia, C. Gualandi, A. Zucchelli, M.L. Focarete, Biomimetic hierarchically arranged nanofibrous structures resembling the architecture and the passive mechanical properties of skeletal muscles: a step forward toward artificial muscle, Front. Boengineering Biotechnol. 8 (2020) 767. https://doi.org/10.3389/fbioe.2020.00767.

[7] A. Sensini, L. Cristofolini, A. Zucchelli, M.L. Focarete, C. Gualandi, A. de Mori, A.P. Kao, M. Roldo, G. Blunn, G. Tozzi, Hierarchical electrospun tendon-ligament bioinspired scaffolds induce changes in fibroblasts morphology under static and dynamic conditions, J. Microsc. 277 (2020) 160–169. https://doi.org/10.1111/jmi.12827.

[8] B. Kong, R. Liu, J. Guo, L. Lu, Q. Zhou, Y. Zhao, Tailoring micro/nano-fibers for biomedical applications, Bioact. Mater. 19 (2023) 328–347. https://doi.org/10.1016/j.bioactmat.2022.04.016.

[9] S. Wu, B. Duan, P. Liu, C. Zhang, X. Qin, J.T. Butcher, Fabrication of aligned nanofiber polymer yarn networks for anisotropic soft tissue scaffolds, ACS Appl. Mater. Interfaces. 8 (2016) 16950–16960. https://doi.org/10.1021/acsami.6b05199.

[10] P. Mouthuy, N. Zargar, O. Hakimi, E. Lostis, A. Carr, Fabrication of continuous electrospun filaments with potential for use as medical fibres, Biofabrication. 7 (2015) 025006. https://doi.org/10.1088/1758-5090/7/2/025006.

[11] M. Aleemardani, A. Solouk, S. Akbari, M.M. Dehghan, M. Moeini, Silk-derived oxygen-generating electrospun patches for enhancing tissue regeneration: Investigation of calcium peroxide role and its effects on controlled oxygen delivery, Materialia. 14 (2020) 100877. https://doi.org/10.1016/j.mtla.2020.100877.

[12] A. Sensini, L. Cristofolini, Biofabrication of electrospun scaffolds for the

regeneration of tendons and ligaments, Materials (Basel). 11 (2018) 1963. https://doi.org/10.3390/ma11101963.

[13] A. Sensini, G. Massafra, C. Gotti, A. Zucchelli, L. Cristofolini, Tissue engineering for the insertions of tendons and ligaments: An overview of electrospun biomaterials and structures, Front. Bioeng. Biotechnol. 9 (2021) 1–23. https://doi.org/10.3389/fbioe.2021.645544.

[14] D.A. Brennan, A.A. Conte, G. Kanski, S. Turkula, X. Hu, M.T. Kleiner, V. Beachley, Mechanical considerations for electrospun nanofibers in tendon and ligament repair, Adv. Healthcare Mater. 7 (2018) 1–31. https://doi.org/10.1002/adhm.201701277.

[15] L.A. Bosworth, N. Alam, J.K. Wong, S. Downes, Investigation of 2D and 3D electrospun scaffolds intended for tendon repair, J. Mater. Sci.: Mater. Med. 24 (2013) 1605–1614. https://doi.org/10.1007/s10856-013-4911-8.

[16] Q. Yang, L. Jianfeng, W. Su, Y. Liu, T. Li, Y. Wang, K. Zhang, Y. WU, L. WANG, Electrospun aligned poly (ε-caprolactone) nanofiber yarns guiding 3D organization of tendon stem/progenitor cells in tenogenic differentiation and tendon repair, Front. Bioeng. Biotechnol. 10 (2022).

[17] L.A. Bosworth, S.R. Rathbone, R.S. Bradley, S.H. Cartmell, Dynamic loading of electrospun yarns guides mesenchymal stem cells towards a tendon lineage, J. Mech. Behav. Biomed. Mater. 39 (2014) 175–183. https://doi.org/10.1016/j.jmbbm.2014.07.009.

[18] L.A. Bosworth, Travelling along the clinical roadmap: developing electrospun scaffolds for tendon repair, Conf. Pap. Sci. 2014 (2014) 1–6. https://doi.org/10.1155/2014/304974.

[19] H.M. Pauly, D.J. Kelly, K.C. Popat, N.A. Trujillo, N.J. Dunne, H.O. McCarthy, T.L. Haut Donahue, Mechanical properties and cellular response of novel electrospun nanofibers for ligament tissue engineering: Effects of orientation and geometry, J. Mech. Behav. Biomed. Mater. 61 (2016) 258–270. https://doi.org/10.1016/j.jmbbm.2016.03.022.

[20] A. Sensini, C. Gualandi, L. Cristofolini, G. Tozzi, M. Dicarlo, G. Teti, M. Mattioli-belmonte, L. Focarete, Biofabrication of bundles of poly(lactic acid)-collagen blends mimicking the fascicles of the human Achille tendon, Biofabrication. 9 (2017) 015025.

[21] A. Sensini, C. Gualandi, A. Zucchelli, L.A. Boyle, A.P. Kao, G.C. Reilly, G. Tozzi, L. Cristofolini, M.L. Focarete, Tendon fascicle-inspired nanofibrous scaffold of polylactic acid/collagen with enhanced 3D-structure and biomechanical properties, Sci. Rep. 8 (2018) 1–15. https://doi.org/10.1038/s41598-018-35536-8.

[22] A. Sensini, M.H. Santare, E. Eichenlaub, E. Bloom, C. Gotti, A. Zucchelli, L. Cristofolini, Tuning the structure of nylon 6,6 electrospun bundles to mimic the mechanical performance of tendon fascicles, Front. Bioeng. Biotechnol. 9 (2021) 1–12. https://doi.org/10.3389/fbioe.2021.626433.

[23] A. Sensini, C. Gualandi, M.L. Focarete, J. Belcari, A. Zucchelli, L. Boyle, G.C. Reilly, A.P. Kao, G. Tozzi, L. Cristofolini, Multiscale hierarchical bioresorbable scaffolds for the regeneration of tendons and ligaments, Biofabrication. 11 (2019) 35026. https://doi.org/10.1088/1758-5090/ab20ad.

[24] S. Camarero-Espinosa, H. Yuan, P.J. Emans, L. Moroni, Mimicking the graded wavy structure of the anterior cruciate ligament, Adv. Healthcare Mater. 2203023 (2023) 2203023. https://doi.org/10.1002/adhm.202203023.

[25] M. Laranjeira, R.M.A. Domingues, R. Costa-Almeida, R.L. Reis, M.E. Gomes, 3D mimicry of native-tissue-fiber architecture guides tendon-derived cells and adipose stem cells into artificial tendon constructs, Small. 13 (2017) 1700689. https://doi.org/10.1002/smll.201700689.

[26] A.T. Speidel, P.R.A. Chivers, C.S. Wood, D.A. Roberts, I.P. Correia, A.S. Caravaca, Y.K.V. Chan, C.S. Hansel, J. Heimgärtner, E. Müller, J. Ziesmer, G.A. Sotiriou, P.S. Olofsson, M.M. Stevens, Tailored biocompatible polyurethane-poly(ethylene glycol) hydrogels as a versatile nonfouling biomaterial, Adv. Healthcare Mater. (2022). https://doi.org/10.1002/adhm.202201378.

[27] A. Shaabani, R. Sedghi, Synthesis of shape memory electroconductive

polyurethane with self-healing capability as an intelligent biomedical scaffold for bone tissue engineering, Polymer (Guildf). 223 (2021) 123694. https://doi.org/10.1016/j.polymer.2021.123694.

[28] S. Bahrami, A. Solouk, H. Mirzadeh, A.M. Seifalian, Electroconductive polyurethane/graphene nanocomposite for biomedical applications, Composites, Part B. 168 (2019) 421–431. https://doi.org/10.1016/j.compositesb.2019.03.044.

[29] S. Bahrami, A. Solouk, D. Duprez, H. Mirzadeh, Microstructure manipulation of polyurethane-based macromolecular scaffold for tendon/ligament tissue engineering, Macromol. Mater. Eng. (2021) 2100584.

[30] C.A. Reznikoff, D.W. Brankow, C. Heidelberger, Establishment and Characterization of a Cloned Line of C3H Mouse Embryo Cells Sensitive to Postconfluence Inhibition of Division, Cancer Res. 33 (1973) 3231–3238.

[31] S.B. Orr, A. Chainani, K.J. Hippensteel, A. Kishan, C. Gilchrist, N.W. Garrigues, D.S. Ruch, F. Guilak, D. Little, Aligned multilayered electrospun scaffolds for rotator cuff tendon tissue engineering, Acta Biomater. 24 (2015) 117–126. https://doi.org/10.1016/j.actbio.2015.06.010.

[32] T.D. Schmittgen, K.J. Livak, Analyzing real-time PCR data by the comparative CT method, Nat. Protoc. 3 (2008) 1101–1108. https://doi.org/10.1038/nprot.2008.73.

[33] S. Wu, R. Zhou, F. Zhou, P.N. Streubel, S. Chen, B. Duan, Electrospun thymosin Beta-4 loaded PLGA/PLA nanofiber/microfiber hybrid yarns for tendon tissue engineering application, Mater. Sci. Eng. C. 106 (2020) 110268. https://doi.org/10.1016/j.msec.2019.110268.

[34] J. Lin, W. Zhou, S. Han, V. Bunpetch, K. Zhao, C. Liu, Z. Yin, H. Ouyang, Cell-material interactions in tendon tissue engineering, Acta Biomater. 70 (2018) 1–11. https://doi.org/10.1016/j.actbio.2018.01.012.

[35] L.T.H. Nguyen, S. Liao, C.K. Chan, S. Ramakrishna, Enhanced osteogenic differentiation with 3D electrospun nanofibrous scaffolds, Nanomedicine. 7

(2012) 1561–1575. https://doi.org/10.2217/nnm.12.41.

[36] W. Han, J. Zhao, M. Tu, R. Zeng, Z. Zha, C. Zhou, Preparation and characterization of nanohydroxyapatite strengthening nanofibrous poly(L-lactide) scaffold for bone tissue engineering, J. Appl. Polym. Sci. 128 (2013) 1332–1338. https://doi.org/10.1002/app.38177.

[37] M. Zhu, R. Zhang, Z. Mao, J. Fang, F. Ren, Topographical biointerface regulating cellular functions for bone tissue engineering, Biosurface and Biotribology. (2022) 165–187. https://doi.org/10.1049/bsb2.12043.

[38] B. Khabbaz, A. Solouk, H. Mirzadeh, Polyvinyl alcohol/soy protein isolate nanofibrous patch for wound-healing applications, Prog. Biomater. 8 (2019) 185–196. https://doi.org/10.1007/s40204-019-00120-4.

[39] S. Deepthi, K. Jeevitha, M. Nivedhitha Sundaram, K.P. Chennazhi, R. Jayakumar, Chitosan-hyaluronic acid hydrogel coated poly(caprolactone) multiscale bilayer scaffold for ligament regeneration, Chem. Eng. J. 260 (2015) 478–485. https://doi.org/10.1016/j.cej.2014.08.106.

[40] M. Xu, T. Su, X. Jin, Y. Li, Y. Yao, K. Liu, K. Chen, F. Lu, Y. He, Inflammation-mediated matrix remodeling of extracellular matrix-mimicking biomaterials in tissue engineering and regenerative medicine, Acta Biomater. 151 (2022) 106–117. https://doi.org/10.1016/j.actbio.2022.08.015.

[41] Y. Wu, Y. Han, Y.S. Wong, J. Ying, H. Fuh, Fiber-based scaffolding techniques for tendon tissue engineering, J. Tissue Eng. Regener. Med. 12 (2018) 1798–1821. https://doi.org/10.1002/term.2701.

[42] S.H. Liu, H.G. Zhang, Q.X. Hu, B. Wang, S. Li, C. Zhang, Development and evaluation of biomimetic 3D coated composite scaffold for application as skin substitutes, Macromol. Mater. Eng. 305 (2020) 1–13. https://doi.org/10.1002/mame.201900848.

[43] D. Gupta, J. Venugopal, M.P. Prabhakaran, V.R.G. Dev, S. Low, A. Tar, S. Ramakrishna, Aligned and random nanofibrous substrate for the in vitro culture of Schwann cells for neural tissue engineering, Acta Biomater. 5 (2009) 2560–

2569. https://doi.org/10.1016/j.actbio.2009.01.039.

[44] Y. Hu, L. Liu, W. Dan, N. Dan, Z. Gu, X. Yu, Synergistic effect of carbodiimide and dehydrothermal crosslinking on acellular dermal matrix, Int. J. Biol. Macromol. 55 (2013) 221–230. https://doi.org/10.1016/j.ijbiomac.2013.01.009.

[45] B.M. Baker, A.O. Gee, R.B. Metter, A.S. Nathan, R.A. Marklein, J.A. Burdick, R.L. Mauck, The potential to improve cell infiltration in composite fiber-aligned electrospun scaffolds by the selective removal of sacrificial fibers, Biomaterials. 29 (2008) 2348–2358. https://doi.org/10.1016/j.biomaterials.2008.01.032.

[46] P.S. Thayer, A.F. Dimling, D.S. Plessl, M.R. Hahn, S.A. Guelcher, L.A. Dahlgren, A.S. Goldstein, Cellularized cylindrical fiber/hydrogel composites for ligament tissue engineering, Biomacromolecules. 15 (2014) 75–83. https://doi.org/10.1021/bm4013056.

[47] Z. Eivazi, A. Solouk, M. Shafieian, M. Haghbin, Electrospun polyurethane/carbon nanotube composites with different amounts of carbon nanotubes and almost the same fiber diameter for biomedical applications, Mater. Sci. Eng. C. 118 (2021) 111403. https://doi.org/10.1016/j.msec.2020.111403.

[48] A.J. Lomas, C.N.M. Ryan, A. Sorushanova, N. Shologu, A.I. Sideri, V. Tsioli, G.C. Fthenakis, A. Tzora, I. Skoufos, L.R. Quinlan, G. O'Laighin, A.M. Mullen, J.L. Kelly, S. Kearns, M. Biggs, A. Pandit, D.I. Zeugolis, The past, present and future in scaffold-based tendon treatments, Adv. Drug Delivery Rev. 84 (2015) 257–277. https://doi.org/10.1016/j.addr.2014.11.022.

[49] S. Wong, A. Baji, S. Leng, Effect of fiber diameter on tensile properties of electrospun poly(ε-caprolactone), Polymer (Guildf). 49 (2008) 4713–4722. https://doi.org/10.1016/j.polymer.2008.08.022.

[50] Q.P. Le, M. V. Uspenskaya, R.O. Olekhnovich, M.A. Baranov, The mechanical properties of PVC nanofiber mats obtained by electrospinning, Fibers. 9 (2021) 1–12. https://doi.org/10.3390/fib9010002.

[51] C. Yang, G. Deng, W. Chen, X. Ye, X. Mo, A novel electrospun-aligned nanoyarn-reinforced nanofibrous scaffold for tendon tissue engineering, Colloids Surf., B.

122 (2014) 270–276. https://doi.org/10.1016/j.colsurfb.2014.06.061.

[52] C. Rinoldi, A. Fallahi, I.K. Yazdi, J. Campos Paras, E. Kijeńska-Gawrońska, G. Trujillo-De Santiago, A. Tuoheti, D. Demarchi, N. Annabi, A. Khademhosseini, W. Swieszkowski, A. Tamayol, Mechanical and biochemical stimulation of 3D multilayered scaffolds for tendon tissue engineering, ACS Biomater. Sci. Eng. 5 (2019) 2953–2964. https://doi.org/10.1021/acsbiomaterials.8b01647.

[53] S. Deepthi, M.N. Sundaram, J.D. Kadavan, R. Jayakumar, Layered chitosan-collagen hydrogel/aligned PLLA nanofiber construct for flexor tendon regeneration, Carbohydr. Polym. 153 (2016) 492–500. https://doi.org/10.1016/j.carbpol.2016.07.124.

[54] S. Gu, B. Yan, L. Liu, J. Ren, Carbon nanotube-polyurethane shape memory nanocomposites with low trigger temperature, Eur. Polym. J. 49 (2013) 3867–3877. https://doi.org/10.1016/j.eurpolymj.2013.10.007.

[55] A.D. Doyle, N. Carvajal, A. Jin, K. Matsumoto, K.M. Yamada, Local 3D matrix microenvironment regulates cell migration through spatiotemporal dynamics of contractility-dependent adhesions, Nat. Commun. 6 (2015). https://doi.org/10.1038/ncomms9720.

[56] Y. Ti, Q. Wen, D. Chen, Characterization of the hydrogen bond in polyurethane/attapulgite nanocomposites, J. Appl. Polym. Sci. 133 (2016) 1–7. https://doi.org/10.1002/app.43069.

[57] F. Guilak, D.M. Cohen, B.T. Estes, J.M. Gimble, W. Liedtke, C.S. Chen, Control of stem cell fate by physical interactions with the extracellular matrix, Cell Stem Cell. 5 (2009) 17–26. https://doi.org/10.1016/j.stem.2009.06.016.

[58] Q. Ma, L. Yang, Z. Jiang, Q. Song, M. Xiao, D. Zhang, X. Ma, T. Wen, G. Cheng, Three-dimensional stiff graphene scaffold on neural stem cells behavior, ACS Appl. Mater. Interfaces. 8 (2016) 34227–34233. https://doi.org/10.1021/acsami.6b12305.

[59] S. Fusco, V. Panzetta, V. Embrione, P.A. Netti, Crosstalk between focal adhesions and material mechanical properties governs cell mechanics and functions, Acta

Biomater. 23 (2015) 63–71. https://doi.org/10.1016/j.actbio.2015.05.008.

[60] G. Kerch, M. Chausson, S. Gautier, R. Merijs Meri, J. Zicans, E. Jakobsons, M. Joner, G. Kerch Riga, Heparin-like polyelectrolyte multilayer coatings based on fungal sulfated chitosan decrease platelet adhesion due to the increased hydration and reduced stiffness, Biomater. Tissue Technol. 1 (2017) 1–5. https://doi.org/10.15761/BTT.1000102.

[61] E. Türker, Ü.H. Yildiz, A. Arslan Yildiz, Biomimetic hybrid scaffold consisting of co-electrospun collagen and PLLCL for 3D cell culture, Int. J. Biol. Macromol. 139 (2019) 1054–1062. https://doi.org/10.1016/j.ijbiomac.2019.08.082.

[62] K.C. Kavya, R. Jayakumar, S. Nair, K.P. Chennazhi, Fabrication and characterization of chitosan/gelatin/nSiO2 composite scaffold for bone tissue engineering, Int. J. Biol. Macromol. 59 (2013) 255–263. https://doi.org/10.1016/j.ijbiomac.2013.04.023.

[63] C. Sun, X. Jin, J.M. Holzwarth, X. Liu, J. Hu, M.J. Gupte, Y. Zhao, P.X. Ma, Development of channeled nanofibrous scaffolds for oriented tissue engineering, Macromol. Biosci. 12 (2012) 761–769. https://doi.org/10.1002/mabi.201200004.

[64] C. Erisken, X. Zhang, K.L. Moffat, W.N. Levine, H.H. Lu, Scaffold fiber diameter regulates human tendon fibroblast growth and differentiation, Tissue Eng., Part A. 19 (2013) 519–528. https://doi.org/10.1089/ten.tea.2012.0072.

[65] J. Ballester-Beltrán, M.J.P. Biggs, M.J. Dalby, M. Salmerón-Sánchez, A. Leal-Egaña, Sensing the difference: The influence of anisotropic cues on cell behavior, Front. Mater. 2 (2015) 1–12. https://doi.org/10.3389/fmats.2015.00039.

[66] S. Sankar, C.S. Sharma, S.N. Rath, S. Ramakrishna, Electrospun fibers for recruitment and differentiation of stem cells in regenerative medicine, Biotechnol. J. 12 (2017) 1700263.

[67] D. Schulz Torres, T.M. Freyman, I. V. Yannas, M. Spector, Tendon cell contraction of collagen-GAG matrices in vitro: Effect of cross-linking, Biomaterials. 21 (2000) 1607–1619. https://doi.org/10.1016/S0142-9612(00)00051-X.

[68] G. Jin, R. He, B. Sha, W. Li, H. Qing, R. Teng, F. Xu, Electrospun three-dimensional

aligned nanofibrous scaffolds for tissue engineering, Mater. Sci. Eng. C. 92 (2018) 995–1005. https://doi.org/10.1016/j.msec.2018.06.065.

[69] H. Li, X. Wang, J. Liu, Z. Liu, H. Wang, X. Mo, J. Wu, Nanofiber configuration affects biological performance of decellularized meniscus extracellular matrix incorporated electrospun scaffolds, Biomed. Mater. 16 (2021). https://doi.org/10.1088/1748-605X/ac28a5.

[70] C. Rinoldi, E. Kijeńska, A. Chlanda, E. Choinska, N. Khenoussi, A. Tamayol, A. Khademhosseini, W. Swieszkowski, Nanobead-on-string composites for tendon tissue engineering, J. Mater. Chem. B. 6 (2018) 3116–3127. https://doi.org/10.1039/c8tb00246k.

[71] Z.-Z. Zhang, S.-J. Wang, J.-Y. Zhang, W.-B. Jiang, A.-B. Huang, Y.-S. Qi, J.-X. Ding, X.-S. Chen, D. Jiang, J.-K. Yu, 3D-printed poly (ε-caprolactone) scaffold augmented with mesenchymal stem cells for total meniscal substitution: a 12-and 24-week animal study in a rabbit model, Am. J. Sports Med. 45 (2017) 1497–1511.

[72] B.B. Rothrauff, B.B. Lauro, G. Yang, R.E. Debski, V. Musahl, R.S. Tuan, Braided and stacked electrospun nanofibrous scaffolds for tendon and ligament tissue engineering, Tissue Eng., Part A. 23 (2017) 378–389. https://doi.org/10.1089/ten.tea.2016.0319.

[73] D. Hoffman-Kim, J.A. Mitchel, R. V. Bellamkonda, Topography, cell response, and nerve regeneration, Annu. Rev. Biomed. Eng. 12 (2010) 203. https://doi.org/10.1146/annurev-bioeng-070909-105351.Topography.

[74] A. Islam, T. Mbimba, M. Younesi, O. Akkus, Effects of substrate stiffness on the tenoinduction of human mesenchymal stem cells, Acta Biomater. 58 (2017) 244–253. https://doi.org/10.1016/j.actbio.2017.05.058.

[75] W.Y. Tong, W. Shen, C.W.F. Yeung, Y. Zhao, S.H. Cheng, P.K. Chu, D. Chan, G.C.F. Chan, K.M.C. Cheung, K.W.K. Yeung, Y.W. Lam, Functional replication of the tendon tissue microenvironment by a bioimprinted substrate and the support of tenocytic differentiation of mesenchymal stem cells, Biomaterials. 33 (2012) 7686–7698. https://doi.org/10.1016/j.biomaterials.2012.07.002.

[76] C.L. Gilchrist, D.S. Ruch, D. Little, F. Guilak, Micro-scale and meso-scale architectural cues cooperate and compete to direct aligned tissue formation, Biomaterials. 35 (2014) 10015–10024. https://doi.org/10.1016/j.biomaterials.2014.08.047.

[77] A.R. Tomás, A.I. Goncąlves, E. Paz, P. Freitas, R.M.A. Domingues, M.E. Gomes, Magneto-mechanical actuation of magnetic responsive fibrous scaffolds boosts tenogenesis of human adipose stem cells, Nanoscale. 11 (2019) 18255–18271. https://doi.org/10.1039/c9nr04355a.

[78] H.-J. Jung, M.B. Fisher, S.L.-Y. Woo, Role of biomechanics in the understanding of normal, injured, and healing ligaments and tendons, BMC Sports Sci. Med. Rehabil. 1 (2009) 1–17. https://doi.org/10.1186/1758-2555-1-9.

[79] S. Chaudhury, C. Holland, M.S. Thompson, F. Vollrath, A.J. Carr, Tensile and shear mechanical properties of rotator cuff repair patches, J. Shoulder Elb. Surg. 21 (2012) 1168–1176. https://doi.org/10.1016/j.jse.2011.08.045.

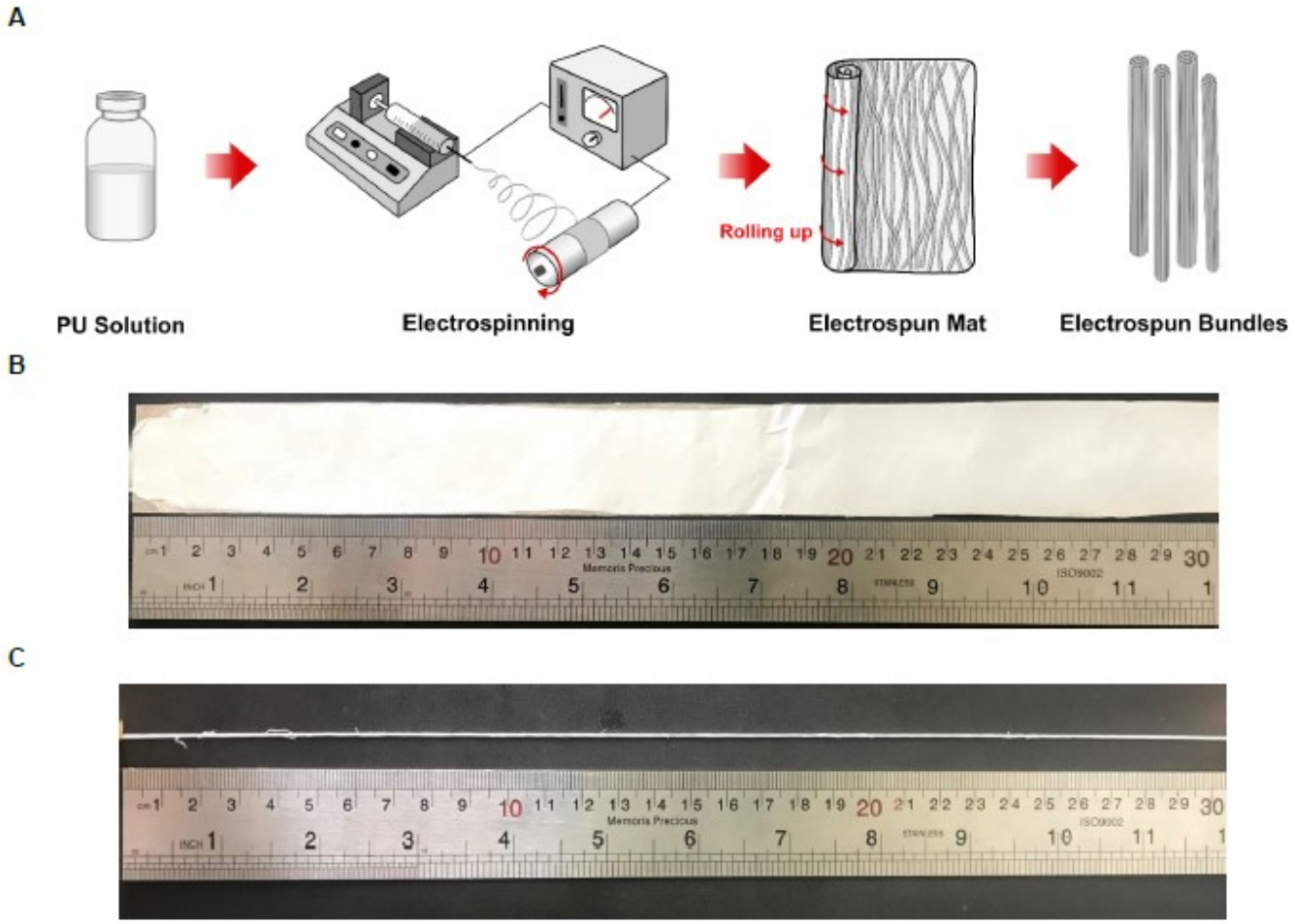

FIGURE 1 Fabrication process of scaffolds. A) Schematic illustration of the stepwise strategy for fabrication of EPU mats and bundles. B) Gross view of the EPU mats. C) Gross view of the EPU bundles.

A

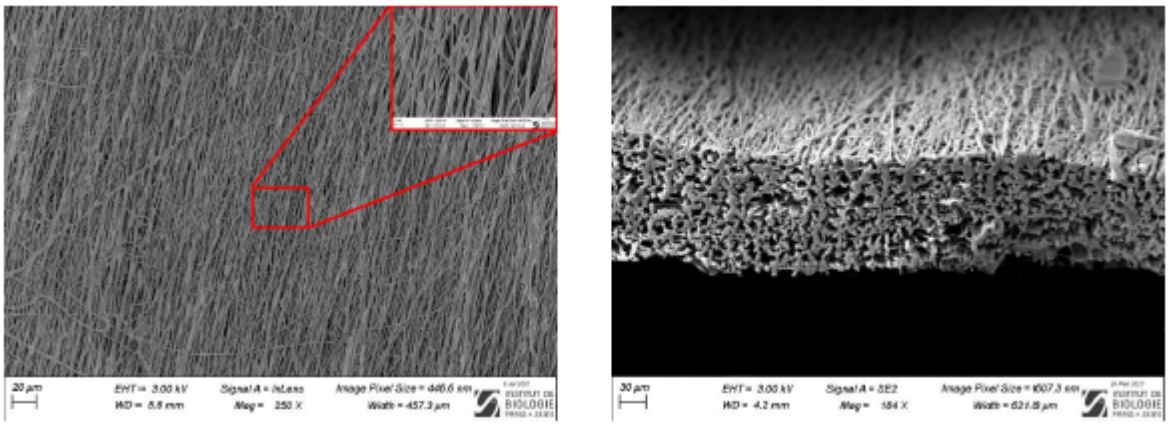

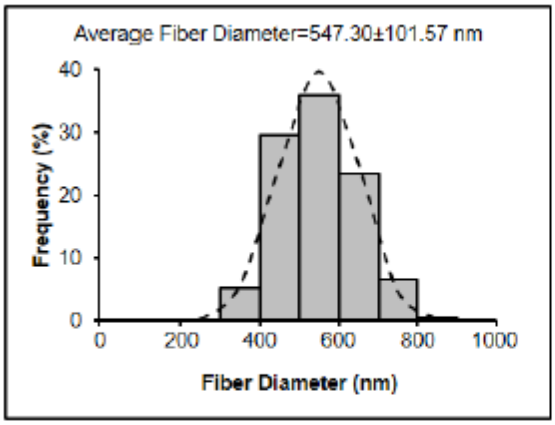

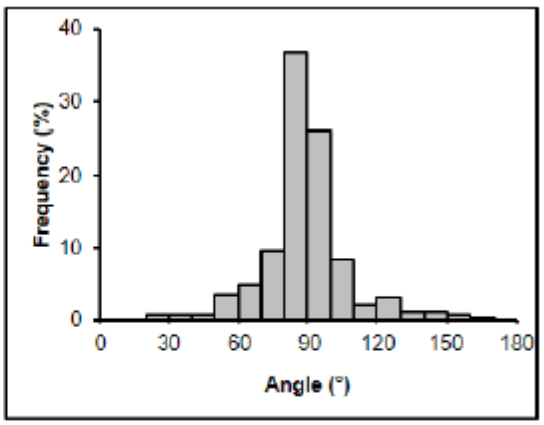

B

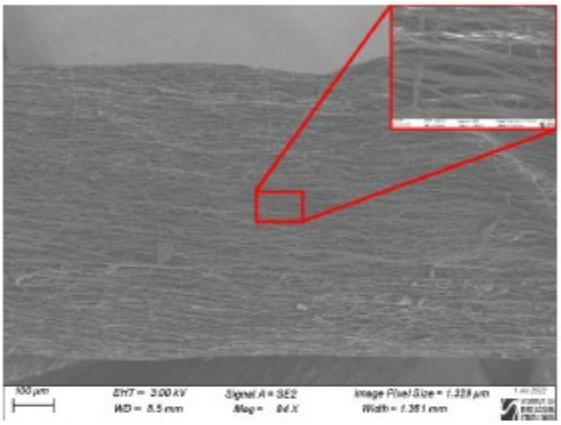

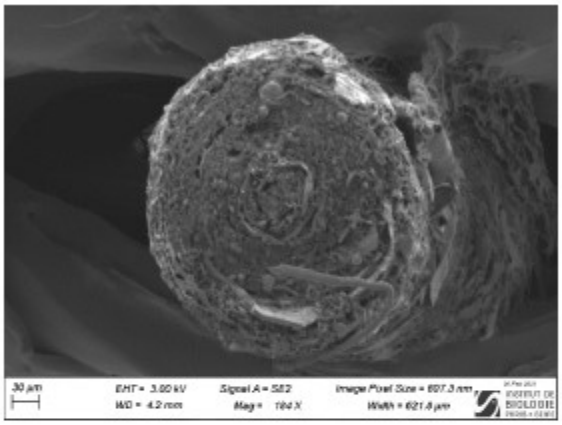

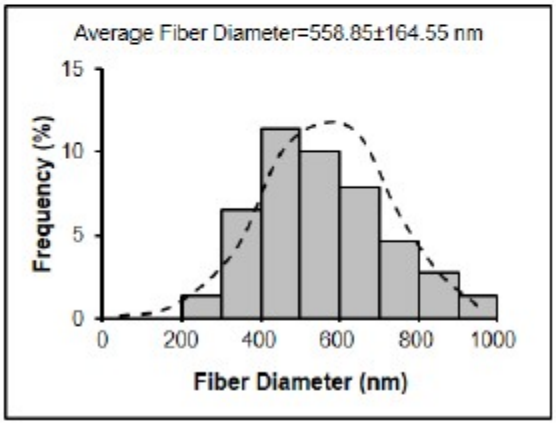

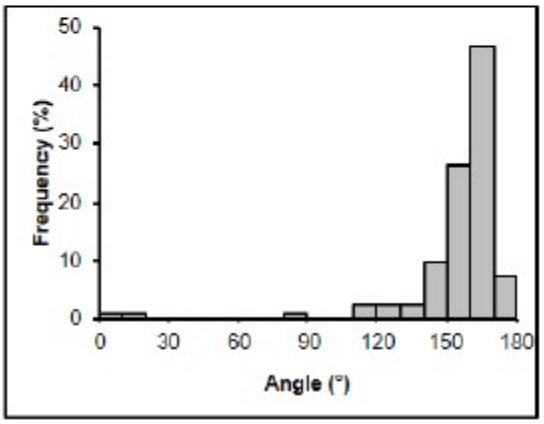

C

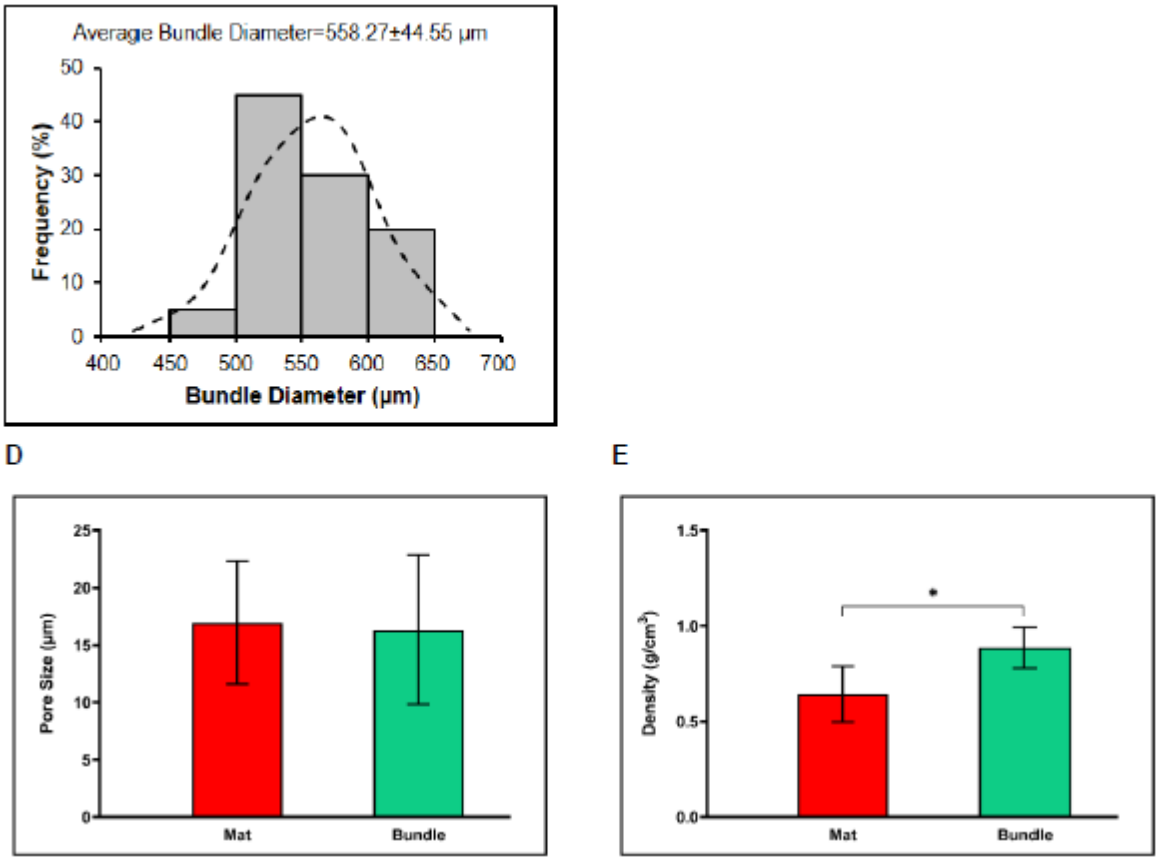

FIGURE 2 Structural characterization of scaffolds. SEM images of A) EPU mat and B) EPU bundle and the corresponding cross-section, distribution of fiber diameter and fiber orientation. C) Distribution of bundle diameter. D) Pore size and E) density of EPU mats and EPU bundles. n = 4-6. *$p < 0.05$.

A

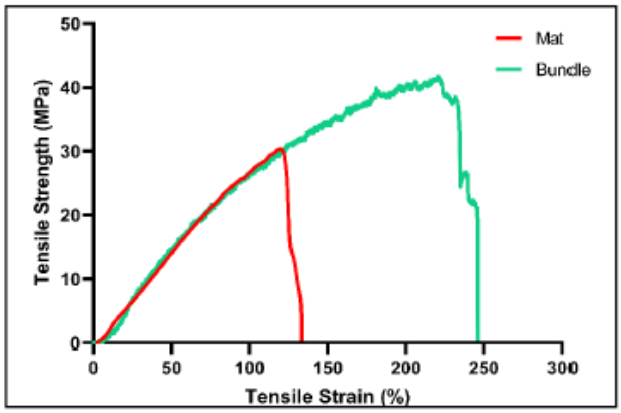

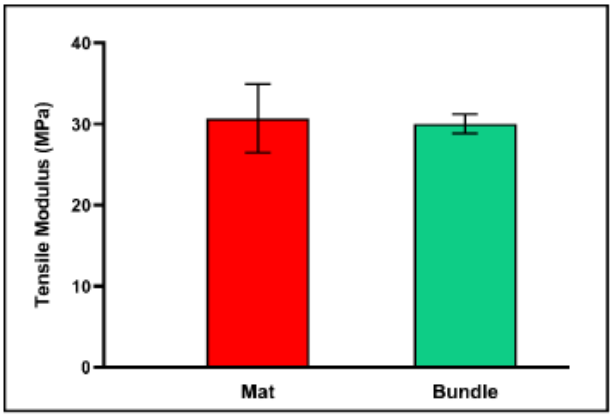

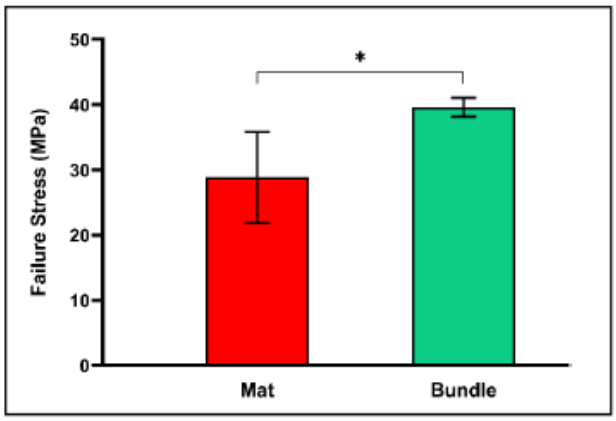

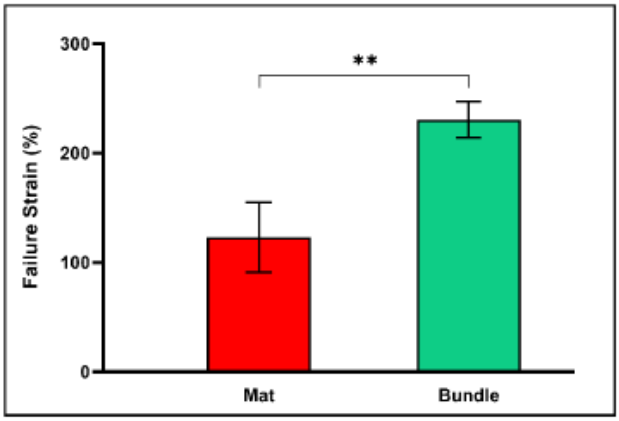

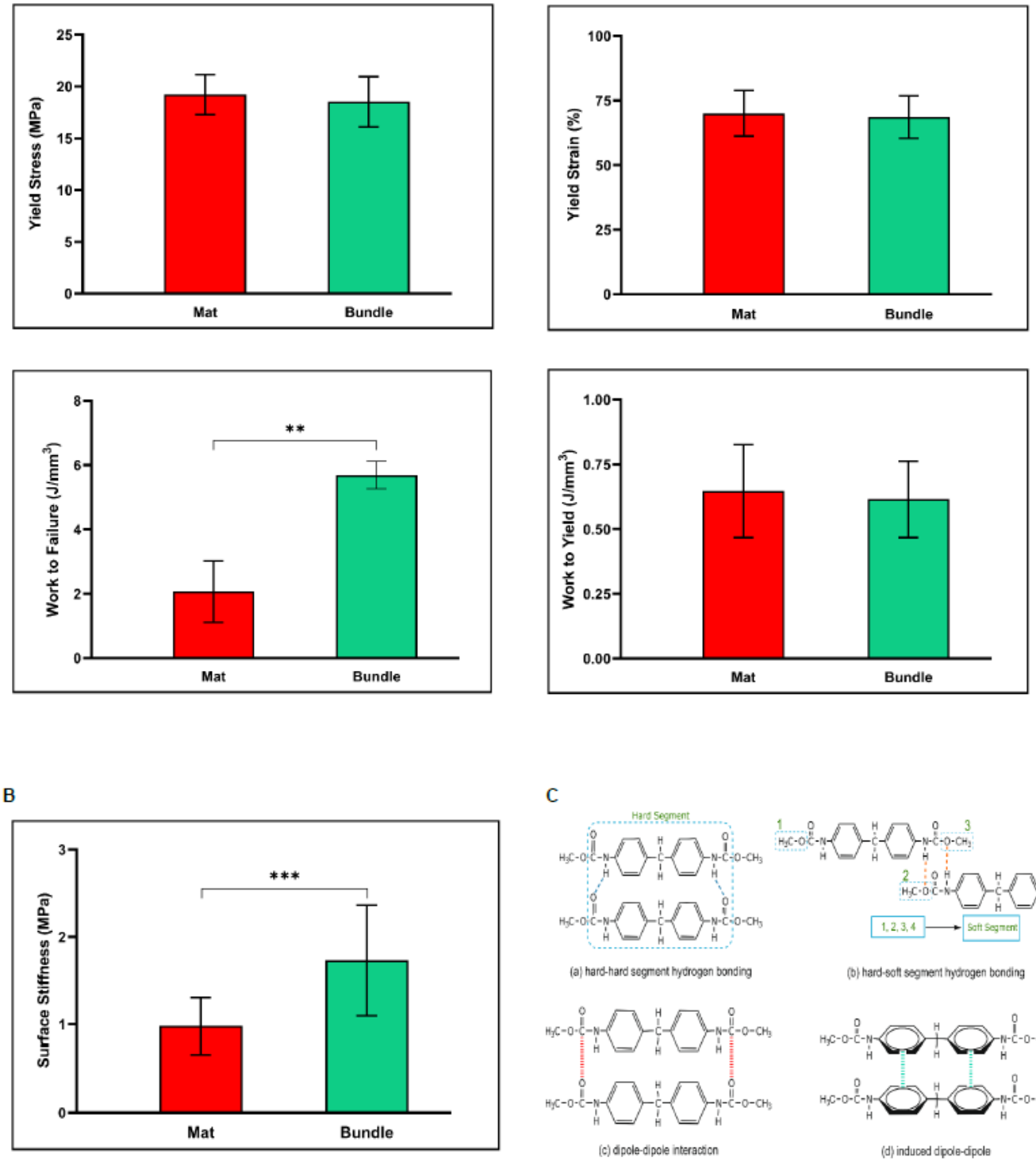

FIGURE 3 Mechanical characterization of scaffolds. A) Typical stress–strain curve of scaffolds and corresponding macroscopic mechanical properties. B) Surface stiffness of scaffolds. At least fifteen different indentations were conducted at different locations on scaffolds surface for each condition. C) Hydrogen bonding and van der Waals forces between polyurethane chains. n = 3-4. *$p < 0.05$, **$p < 0.01$, and ***$p < 0.001$.

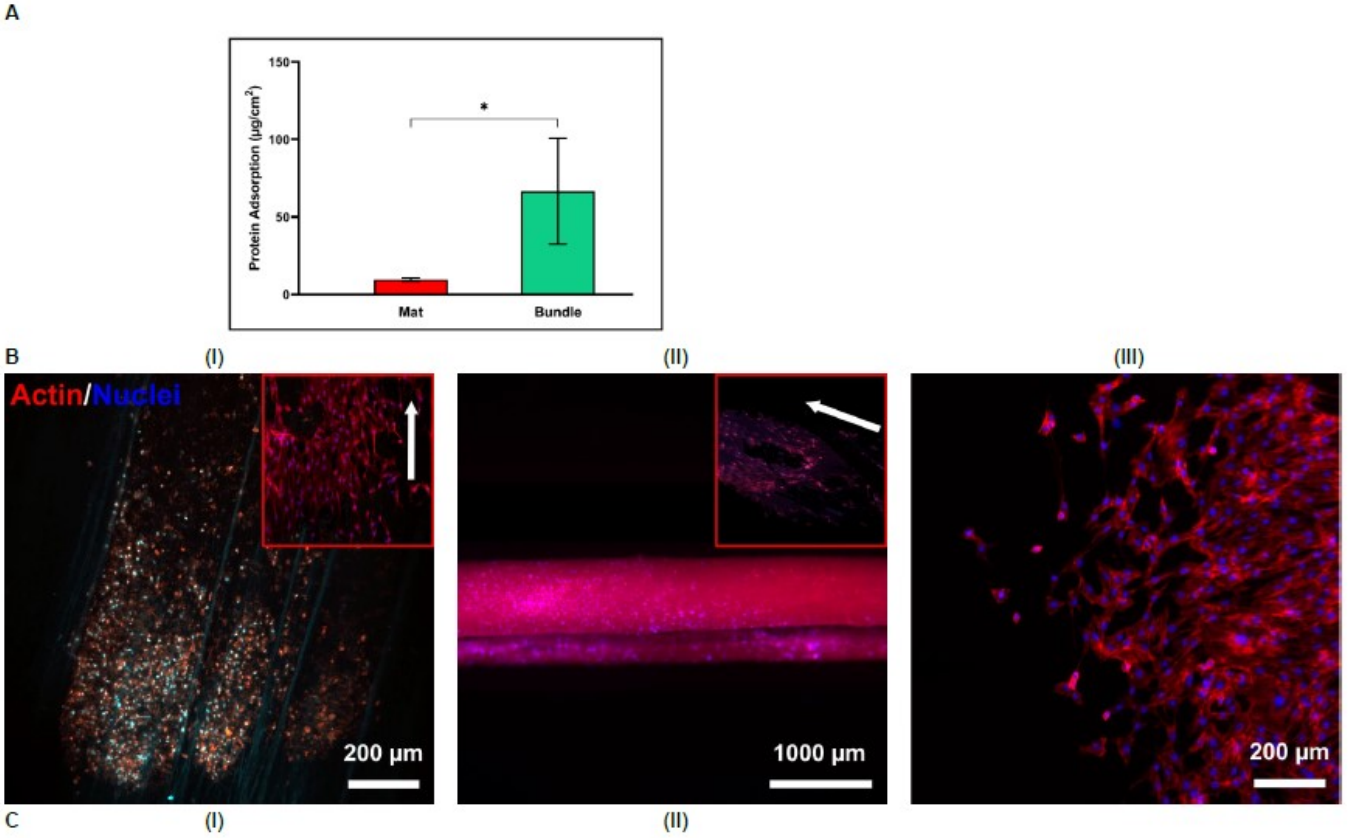

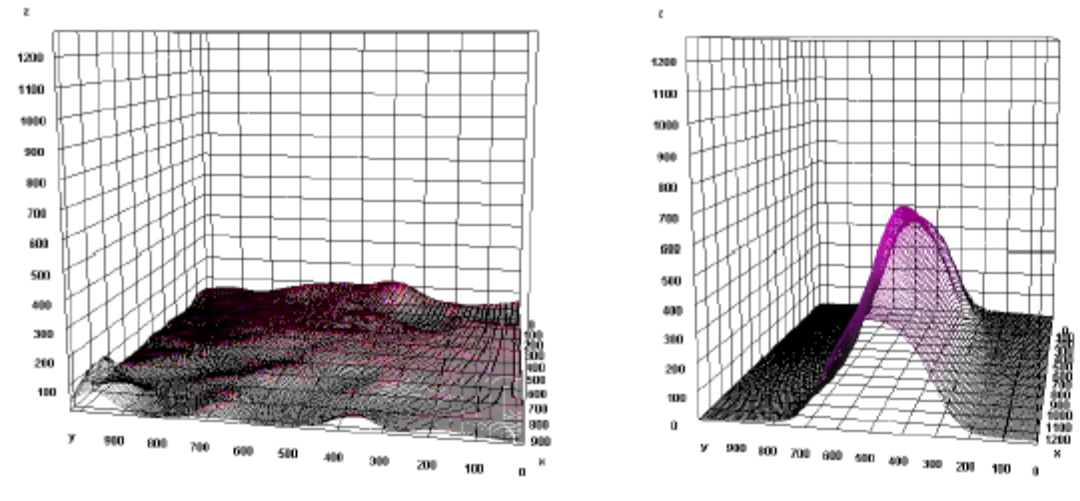

D

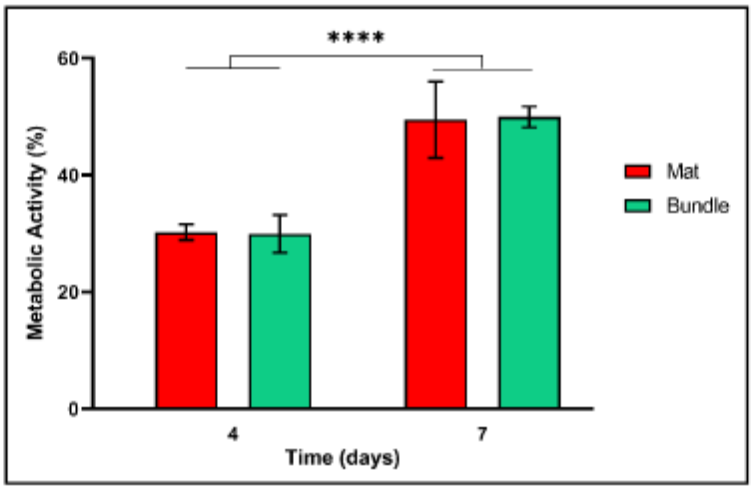

E F G

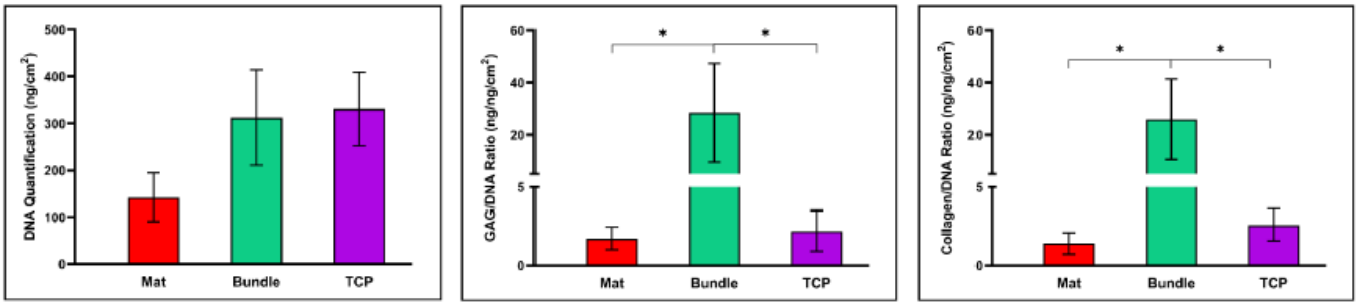

H

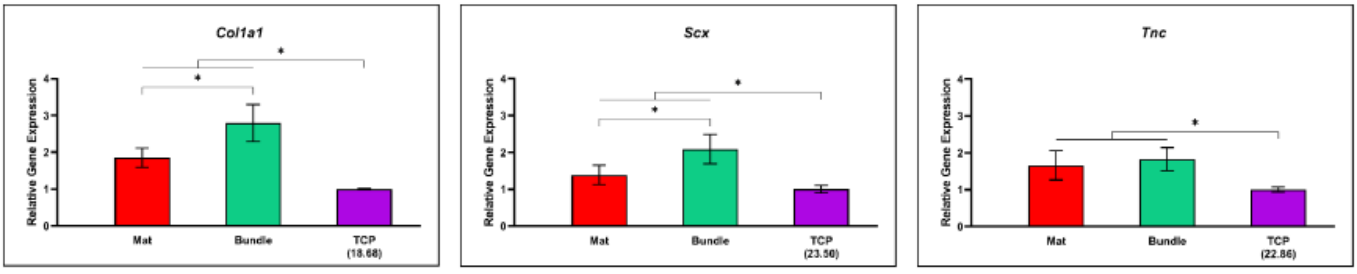

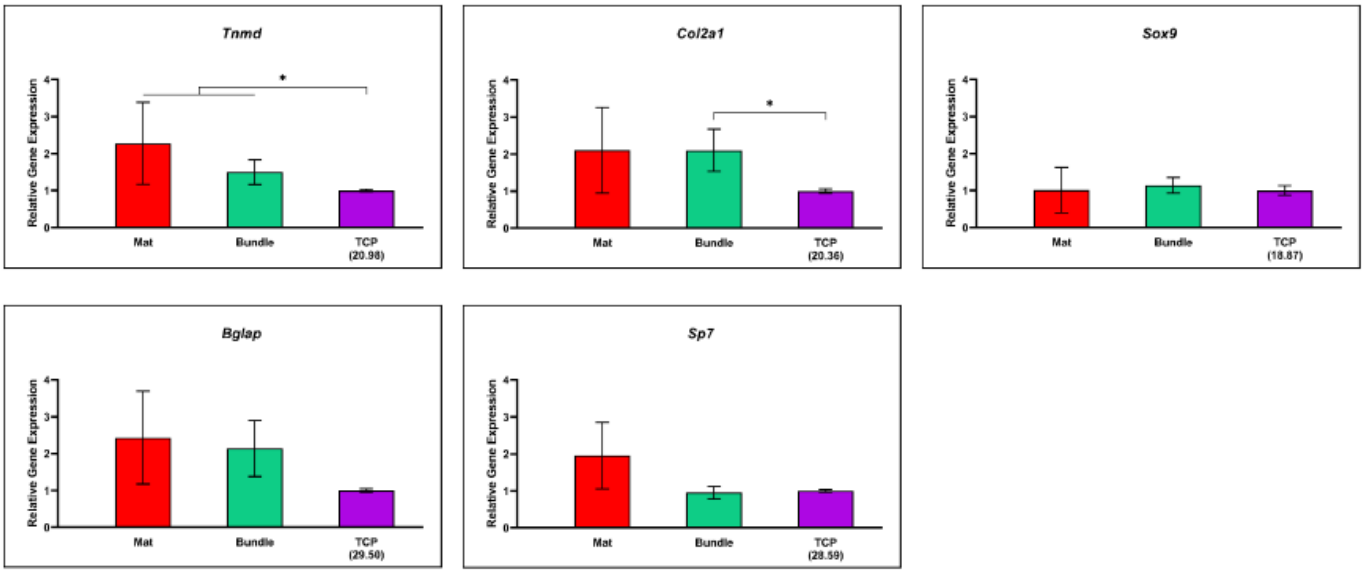

FIGURE 4 Biological evaluation of scaffolds. A) Protein adsorption on the surface of scaffolds. B) Fluorescence images of stained MSCs on the (I) EPU mats, (II) EPU bundles, and (III) TCP (control) after 7 days of culture. Actin fibers and nuclei were stained with phalloidin (red) and DAPI (blue), respectively. C) Distribution of cell infiltration into the (I) EPU mats and (II) EPU bundles after 7 days of culture. Actin fibers and nuclei were stained with phalloidin (red) and DAPI (blue), respectively. The scale of the x-, y-, and z-axis is the micrometer. D) Metabolic activity of MSCs on scaffolds after 7 days of culture using Alamar Blue assay. (E-G) Biochemical composition of cell-seeded samples after 7 days of culture. H) Relative expression of mRNA levels for *Col1a1*, *Scx*, *Tnc*, *Tnmd*, *Col2a1*, *Sox9*, *Bglap* and *Sp7* genes by MSCs after 7 days of culture on different samples. For each gene, the delta threshold cycle (ΔCt) was calculated using *Rn18S* as a reference gene and the expression levels were compared to TCP. For each gene, the mRNA levels of control conditions (TCP) were normalized to 1. The means of the initial threshold cycles (Cts) of TCP (obtained from 500 ng of mRNA) were indicated in brackets. n = 3-4. *$p < 0.05$ and ****$p < 0.0001$.

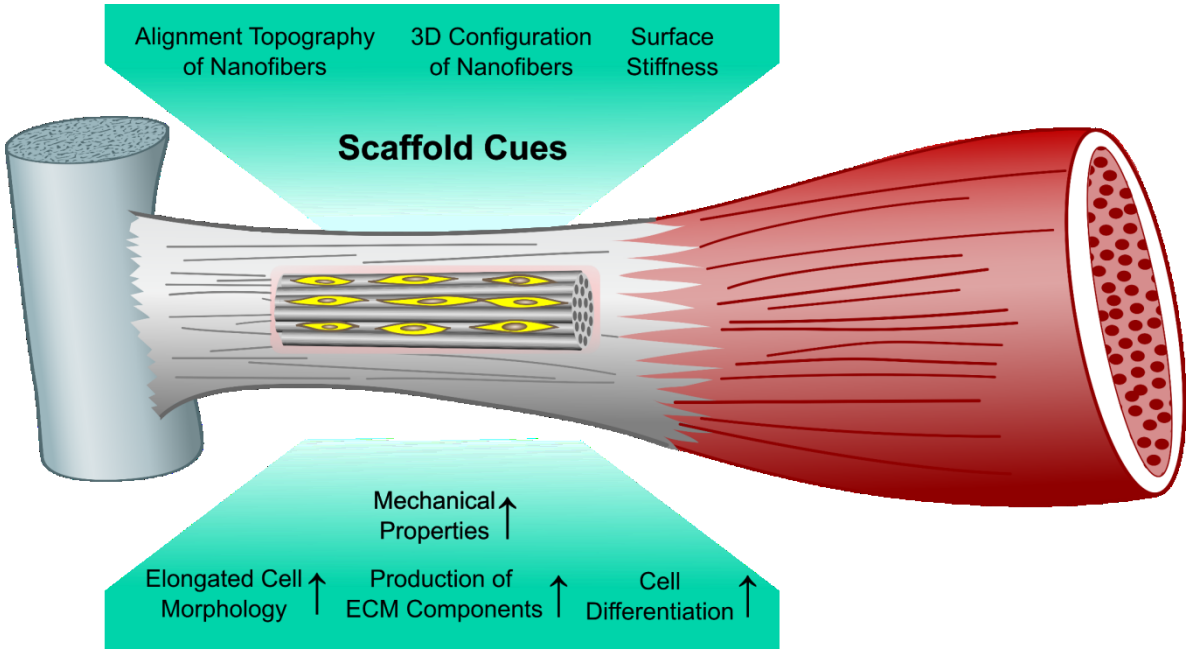

FIGURE 5 Summary of this study.

Table 1. Mechanical properties of samples, native tissues, and commercial graft.

Sample	Tensile Strength (MPa)	Tensile Strain (%)	Reference
EPU mat	29.40±6.14	141.09±37.41	-
EPU bundle	40.38±0.99	259.58±8.81	-
Patellar tendon	54–65	12–15	[78]
Anterior cruciate ligament	13–46	15–44	[78]
Artelon® (SportMesh™)	11.9±4.6	82.0±10.0	[79]

Graphical Abstract and Lay Summary

Hierarchical anisotropy structure directing 3D cellular activities plays a vital role in designing scaffolds for tendon/ligament tissue engineering. To this aim, Polyurethane bundle scaffolds with hierarchically nanofibrous arrangement were developed. The electrospun bundles improved the mechanical properties. They also provided favorable biophysical (alignment topography and 3D configuration of nanofibers) and biomechanical (surface stiffness) cues for tendon/ligament tissue engineering reflected by the promotion of MCS functions including alignment and elongated morphology, ECM components synthesis, and tenogenic differentiation.